Synthesis, Molecular Structures, and Nuclear Magnetic Resonance Properties of the Macropolyhedral Metallaboranes $[(PMe_2Ph)_4Pt_3B_{14}H_{16}]$ and $[(PMe_2Ph)PtB_{16}H_{18}(PMe_2Ph)]$,† and a Discussion of the Bonding at Platinum in These and Some Related Platinaborane Clusters

Michael A. Beckett, Janet E. Crook, Norman N. Greenwood, and John D. Kennedy
Department of Inorganic and Structural Chemistry, University of Leeds, Leeds LS2 9JT

Thermolysis of $[4\text{-}(PMe_2Ph)_2\text{-}arachno\text{-}4\text{-}PtB_8H_{12}]$ in refluxing toluene solution gives the known yellow 14-vertex diplatinaborane $[(PMe_2Ph)_2Pt_2B_{12}H_{18}]$ plus two novel 17-vertex cluster compounds, *viz.* the green triplatinaborane $[(PMe_2Ph)_4Pt_3B_{14}H_{16}]$ (**1**) and the red monoplatinaborane $[(PMe_2Ph)PtB_{16}H_{18}(PMe_2Ph)]$ (**2**). Crystals of (**1**), as its 1:1 solvate with CH_2Cl_2, are monoclinic, space group $P2_1/c$, with a = 1 249.0(3), b = 3·732.6(8), c = 1 072.0(2) pm, β = 104.92(2)°, and Z = 4; the structure was refined using 4 802 independent F_o with $I > 2\sigma(I)$ to a final R = 0.049, R' = 0.045. Crystals of (**2**) are also monoclinic, space group $P2_1$, with a = 992.7(3), b = 1 067.2(2), c = 1 378.7(3) pm, β = 95.08(2)°, and Z = 2; the structure was refined using 1 992 independent F_o with $I > 2\sigma(I)$ to a final R = 0.0216, R' = 0.0248. These two new macropolyhedral boranes have been further characterized by multielement, multiple resonance, and multidimensional n.m.r. spectroscopy. The metal-to-borane bonding is discussed in terms of the 'non-conical' nature of the platinum contribution to the cluster bonding schemes.

The 'conical' isolobal analogy between BH and some transition-metal fragments ML_3 is now widely recognized and, when interpreted in conjunction with simple electron-counting rules,[1–6] has been invaluable in aiding the understanding of polyhedral cluster shapes.[7] However, there is now an increasing number of exceptions to these rules and, in this context, the role of non-conical ML_x fragments in polyhedral cluster compounds is of some theoretical interest.[8,9] Thus, incorrect cluster geometries are sometimes predicted from more traditional electron-counting rules when each vertex of a cluster containing such a fragment is naively assumed to have a predominantly conical character.[10,11] In known polyhedral metallaborane chemistry,[12–17] a non-conical fragment can result from the presence of a metal centre which differs from BH in the number and/or the geometrical arrangement of the orbitals it contributes to the cluster.[16–21] Three categories can be distinguished in which the metal centre has available for cluster bonding: (*i*) four (or more) mutually *cis* orbitals, as in a six-orbital octahedral ML_2 or seven-orbital capped-octahedral or related ML_3 environment [see structures (**I**) and (**II**)]; (*ii*) two orbitals in a *cis* disposition, as in a six-orbital octahedral ML_4 or a four-orbital square-planar ML_2 system [see structures (**III**) and (**IV**)]; and (*iii*) three orbitals in a 'T-shaped' or *mer* configuration, as in a square-planar ML or octahedral ML_3 fragment [see structures (**V**) and (**VI**)]. An example of the first category is *'isocloso'*-$[(PPh_3)_2RuB_{10}H_8(OEt)_2]$, in which the ruthenium atom is believed to contribute four orbitals and four electrons to the cluster-bonding scheme.[18,20–22] An example from the second category is *arachno*-$[6,9\text{-}(S_2CNEt_2)_2\text{-}6,9\text{-}Au_2B_8H_{10}]$, in which the gold atoms at the (6) and (9) vertices are each thought to contribute two orbitals and two electrons to the cluster.[10]

We now describe and discuss a series of macropolyhedral platinaborane cluster compounds which can be considered to exemplify the third category, namely, 'T-shaped' three-orbital contributors. In these compounds certain of the metal-to-borane bonding modes can be interpreted in terms of major contributions involving three metal-centred orbitals which have a 'planar' rather than a 'conical' disposition [structure (**V**)]. Some aspects of the work have been included in preliminary communications.[23–26]

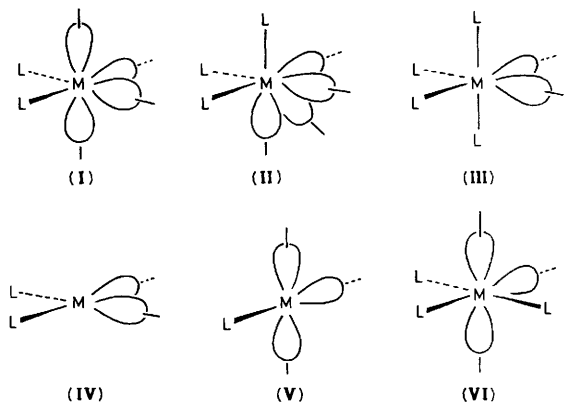

Results and Discussion

(*a*) *Preparation and General Considerations.*—Thermolysis of the *arachno*-type nine-vertex cluster compound $[(PMe_2Ph)_2\text{-}PtB_8H_{12}]$[27] (Figure 1) in refluxing toluene solution yields a number of interesting and novel platinaborane cluster species [equation (1)].

$$\begin{aligned}&[(PMe_2Ph)_2PtB_8H_{12}] \xrightarrow[\text{reflux 1 h}]{\text{toluene}} \\ &[(PMe_2Ph)_4Pt_3B_{14}H_{16}]\ (\mathbf{1};\ \text{green}) \\ &+\ [(PMe_2Ph)PtB_{16}H_{18}(PMe_2Ph)]\ (\mathbf{2};\ \text{red}) \\ &+\ [(PMe_2Ph)_2Pt_2B_{12}H_{18}]\ (\mathbf{3};\ \text{yellow}) \\ &+\ (\mathbf{4}),\ (\mathbf{5}),\ \text{and}\ (\mathbf{6})\ \text{(see later)}\end{aligned} \quad (1)$$

† 2,2,7,10-Tetrakis(dimethylphenylphosphine)-2,7,10-triplatinahepta-decaborane and 7,9′-bis(dimethylphenylphosphine)-7-platinahepta-decaborane respectively.

Supplememtary data available: see Instructions for Authors, *J. Chem. Soc., Dalton Trans.*, 1986, Issue 1, pp. xvii—xx. Structure factors are available from the editorial office.

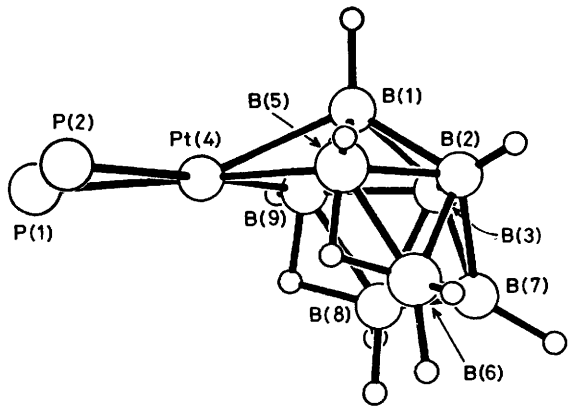

Figure 1. Representation of the molecular structure of the starting nine-vertex *arachno*-metallaborane [4,4-$(PMe_2Ph)_2$-*arachno*-4-PtB_8H_{12}], with P-organyl groups omitted for clarity.[27] In this projection the *exo*-terminal hydrogen atom on B(3) is obscured. The phosphorus atoms P(1) and P(2) are almost exactly *trans* to B(5) and B(9) respectively

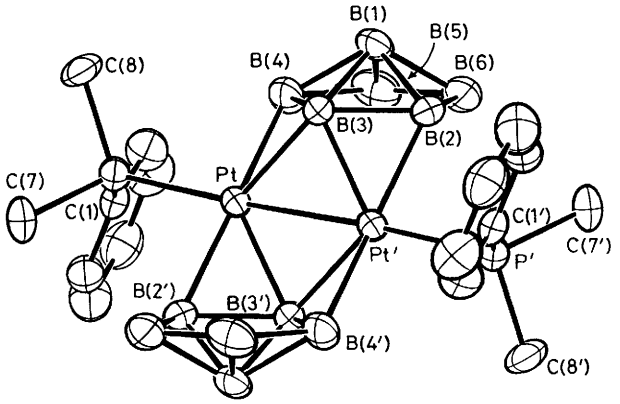

Figure 2. ORTEP Drawing of the molecular structure of the yellow 14-vertex bimetallic product $[(PMe_2Ph)_2Pt_2B_{12}H_{18}]$ (**3**).[28] Hydrogen atoms were not located in the diffraction analysis, but n.m.r. spectroscopy shows that each boron atom has an *exo*-terminal hydrogen atom bound to it, and that there are bridging hydrogen atoms at borane cluster sites (2,6), (4,5), and (5,6)

The highly coloured macropolyhedral cluster compounds (**1**), (**2**), and (**3**) are the main products isolated from the reaction (in yields of 6, 2, and 4% respectively, based on platinum content), and there are some other minor products including (**4**), (**5**), and (**6**) (see later).

Compound (**1**) was obtained as a dark pine-green microcrystalline solid and compound (**2**) as flame red crystals (m.p. 96 °C). Both compounds are air-stable, and are novel 17-vertex species. Compound (**3**), the bright yellow 14-vertex cluster species $[(PMe_2Ph)_2Pt_2B_{12}H_{18}]$ (Figure 2), has been described previously.[28] It is an air-stable solid originally formed in modest yield by the reaction of *cis*-$[PtCl_2(PMe_2Ph)_2]$ with 6,6'-$(B_{10}H_{13})_2O$; it is also a product in a number of other related reaction systems.[27,29,30] Other highly coloured products, *e.g.* compounds (**4**) (red), (**5**) (red-orange), and (**6**) (red-orange) can be separated from the thermolysis mixture, but, unlike (**1**), (**2**), and (**3**), their incidence is erratic and their yields are smaller (< 1%). We have not yet been able to characterize them fully. They are somewhat less stable than (**1**) and (**2**) in solution, but appear to be stable in the solid state. Meanwhile we can report that preliminary multielement n.m.r. spectroscopy shows that these are also novel macropolyhedral platinaboranes, each probably also with *ca.* 17 vertices. Compound (**4**) has four PMe_2Ph ligands, three bound to platinum and one to boron; it readily decomposes to give (**5**) which has one less PMe_2Ph ligand on platinum. Compound (**6**) appears to be an isomer, or near-isomer, of (**5**) also with two phosphines on platinum and one bound to boron, but is formed independently of (**4**) and (**5**). It is not yet known whether these three species have one or two metal atoms per molecule, but all have B–H–B bridging hydrogen atoms. In general, (**4**), (**5**), and (**6**) differ from (**2**) in that this last has only one metal-bound phosphine, although it still retains the cluster-bound phosphine ligand. We hope to be able to report more thoroughly on compounds (**4**), (**5**), and (**6**) at some future date.*

In spite of this variety of novel metallaboranes, the major process of the reaction appears to be one of destructive degradation of the starting platinanonaborane cluster since the reaction is not clean and only *ca.* 15% of the platinum in the starting material appears in the isolable products. A substantial amount of intractable material is formed. Such behaviour is perhaps to be expected when one considers the variety of products obtained and their low yields. It is interesting to note that, whilst decomposition of the starting platinanonaborane cluster occurs, no smaller platinaborane structures have been isolated in this work and only larger metallaborane species have been obtained. Mechanistically this implies a conjoining of a smaller borane or metallaborane fragment about a platinum atom centre of a platinaborane cluster in a regiospecific manner, with the new conjoined polyhedral fragment remaining within the co-ordination sphere of the platinum atom. This behaviour may be compared to the metal-atom-assisted syntheses of the macropolyhedral binary borane anion *anti*-$[B_{18}H_{21}]^-$ in the stoicheiometric reaction of *nido*-$[B_9H_{12}]^-$ with $[\{Os(CO)_3Cl\}_2]$;[31] in this reaction the conjoined borane does not remain co-ordinated to the osmium centre and a macropolyhedral metal-containing species is not formed. Another example is the more recent synthesis of the *conjuncto*-borane $B_{12}H_{16}$ by metal-induced oxidative fusion of *nido*-$[B_6H_9]^-$.[32] The behaviour may also be compared to the thermolysis of the non-metal-containing *arachno* nine-vertex species $B_9H_{13}(SMe_2)$.[33,34] This gives the macropolyhedral species $B_{16}H_{20}$ and $B_{18}H_{22}$ in yields of up to 7 and 20% respectively in the absence of a metal centre, which indicates that the role of the metal centre is not always essential in the conjunction process. It is obviously of undoubted significance in the present reaction, however, since the macropolyhedral platinaborane structures all involve metal atoms at the points of conjunction of the component subclusters [see Figure 5, and sections (*b*) and (*c*) below].

This complex *aufbau* or fusion behaviour which occurs during the thermolysis of the nine-vertex *arachno* species $[(PMe_2Ph)_2PtB_8H_{12}]$ and $B_9H_{13}(SMe_2)$ contrasts to the clean dehydrogenation reaction observed upon thermolysis of the *arachno* nine-vertex iridaborane analogues such as $[(CO)(PMe_3)_2HIrB_8H_{12}]$ under somewhat milder conditions.[35,36] This iridaborane cluster loses one molecule of dihydrogen and forms a *nido* cluster $[(CO)(PMe_3)_2IrB_8H_{11}]$ in quantative yield with first-order kinetics.[36] The difference in behaviour between these two compounds can perhaps be explained in part by the preference of iridium(III) to form octahedral 18-electron complexes, whereas platinum(II) tends to remain a 16-electron species rather than attain the electronic configuration of the next noble gas. Iridium retains an 18-electron configuration and presumably prefers intramolecular redox processes. The 16-electron platinum configuration, however, permits the intermolecular attack (and transient 18-electron species) which

* *Note added in proof.* Compound (**6**) has now been identified by single-crystal *X*-ray structure analysis as $[(PMe_2Ph)_2Pt_2B_{16}H_{15}(C_6H_4Me\text{-}p)(PMe_2Ph)]$: M. A. Beckett, N. N. Greenwood, J. D. Kennedy, P. A. Salter, and M. Thornton-Pett, *J. Chem. Soc., Chem. Commun.*, 1986, 556.

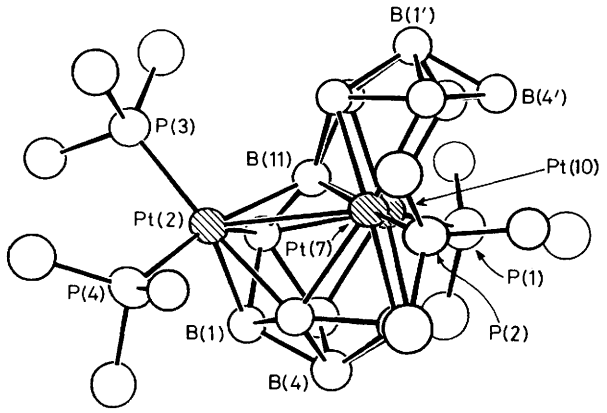

Figure 3. Molecular structure of the green 17-vertex trimetallic compound $[(PMe_2Ph)_4Pt_3B_{14}H_{16}]$ (**1**), with selected organyl carbon atoms omitted for clarity. Hydrogen atoms were not located crystallographically. See Figure 4 for a different orientation

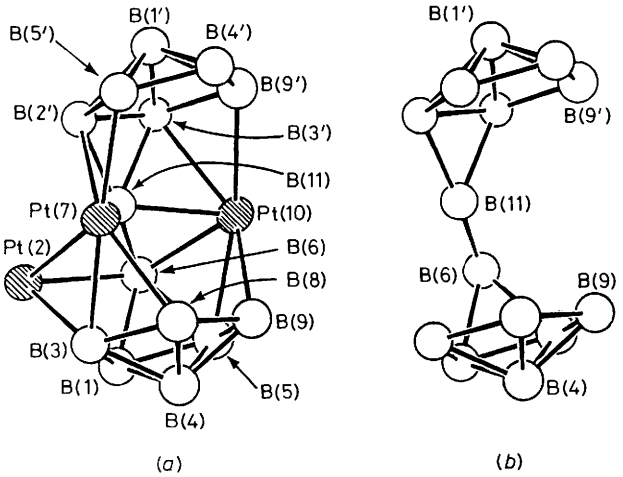

Figure 4. (*a*) View of the Pt_3B_{14} core of (**1**), and (*b*) a view of the B_{14} unit only

would reasonably be part of the macropolyhedral *aufbau* tectonics.

(*b*) *Molecular Structure of* $[(PMe_2Ph)_4Pt_3B_{14}H_{16}]$ (**1**).—An ORTEP drawing of the molecular structure of $[(PMe_2Ph)_4Pt_3B_{14}H_{16}]$ is shown in Figure 3. The heavy-atom cluster geometry can be seen in Figure 4(*a*) and selected interatomic distances and angles are in Tables 1 and 2 respectively. The gross heavy-atom cluster structure comprises a 17-vertex polyhedral configuration with a seven-membered $\overline{PtB_2PtB_3}$ open face [Pt(10), B(9), B(8), Pt(7), B(5'), B(4'), B(9')], but with an otherwise deltahedral framework. The structure can be interpreted in terms of two fused subclusters: (*i*) an *arachno*-type nine-vertex 6',8'-Pt_2B_7 moiety which has its Pt(6')–B(7')–Pt(8') atoms in common with (*ii*) a *nido*-type 11-vertex 2,7,10-Pt_3B_8 moiety distorted somewhat from the idealized $[B_{11}H_{14}]^-$ configuration by the accommodation of the larger platinum atoms. These two subclusters are shown schematically in Figure 5(*a*).

The Pt(2)–Pt(7) interatomic distance of 301.2(1) pm is rather long for a Pt–Pt single bond [*cf.* 264.4(1) pm for compound (**3**),[28] for example] but even at this distance there is likely to be a significant bonding interaction between these two platinum atoms. By contrast, the longer Pt(7)–Pt(10) interatomic

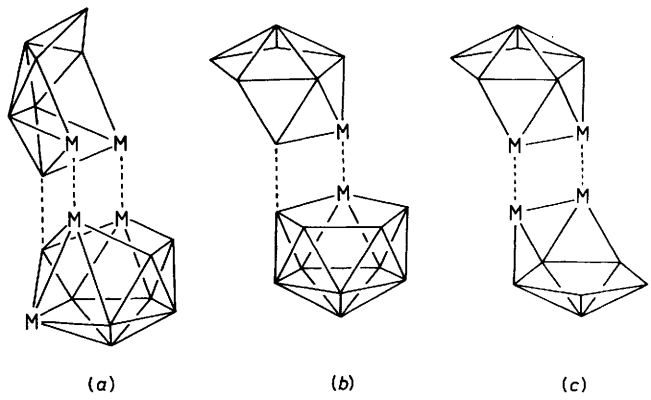

Figure 5. Schematic diagrams of the structural components of (*a*) (**1**) (a fused *nido*-Pt_3B_8/*arachno*-Pt_2B_7 cluster), (*b*) (**2**) (a fused *nido*-PtB_{10}/*arachno*-PtB_7 cluster), and (*c*) (**3**) (two fused *arachno*-Pt_2B_6 clusters)

Table 1. Selected interatomic distances (pm) for $[(PMe_2Ph)_4Pt_3B_{14}H_{16}]$ (**1**) with estimated standard deviations (e.s.d.s) in parentheses

(*a*) Involving platinum atoms			
Pt(7)–Pt(10)	337.6(1)	Pt(7)–Pt(2)	301.2(1)
Pt(2)–P(3)	234.1(4)	Pt(2)–P(4)	232.4(4)
Pt(10)–P(1)	228.8(4)	Pt(7)–P(2)	231.0(4)
Pt(2)–B(1)	223.3(17)	Pt(2)–B(3)	230.8(18)
Pt(2)–B(6)	225.0(16)	Pt(2)–B(11)	218.6(17)
Pt(7)–B(3)	237.9(17)	Pt(7)–B(8)	228.6(18)
Pt(7)–B(11)	212.6(17)	Pt(7)–B(5')	225.7(17)
Pt(7)–B(2')	227.4(17)		
Pt(10)–B(5)	226.5(18)	Pt(10)–B(6)	223.5(17)
Pt(10)–B(9)	228.1(18)	Pt(10)–B(11)	212.3(16)
Pt(10)–B(3')	228.2(15)	Pt(10)–B(9')	230.4(18)
(*b*) Boron–boron			
B(1)–B(3)	187.0(23)	B(3)–B(4)	179.1(23)
B(1)–B(4)	173.1(24)	B(3)–B(8)	184.2(24)
B(1)–B(5)	177.8(24)	B(4)–B(5)	180.7(25)
B(1)–B(6)	187.1(23)	B(4)–B(8)	178.6(24)
B(6)–B(11)	181.0(23)	B(4)–B(9)	175.7(24)
B(5)–B(6)	185.1(24)	B(8)–B(9)	180.6(24)
B(5)–B(9)	182.5(25)	B(11)–B(2')	179.2(22)
B(1')–B(5')	174.7(24)	B(11)–B(3')	182.6(23)
B(1')–B(2')	180.7(22)	B(2')–B(5')	177.8(23)
B(1')–B(3')	182.1(22)	B(4')–B(5')	177.3(24)
B(1')–B(4')	171.2(24)	B(3')–B(2')	184.4(22)
B(1')–B(9')	178.2(24)	B(9')–B(3')	175.9(23)
B(9')–B(4')	179.9(25)		

distance of 337.6(1) pm precludes the possibility of bonding between these two cluster atoms.

The boron–boron distances and interatomic angles in the two pentagonal-pyramidal fragments B(1), B(3), B(4), B(5), B(8), B(9) and B(1'), B(2'), B(3'), B(4'), B(5'), B(9') [see Figure 4(*b*)] are within the normal ranges found in binary borane and metallaborane cluster species.[16,37,38] The central two boron atoms [B(6) and B(11)] together with the three platinum atoms [Pt(2), Pt(7), and Pt(10)] hold the two hexaboranyl fragments in such a manner that the plane defined by the atoms B(2'), B(3'), B(4'), B(5'), B(9'), and the plane containing the atoms B(1), B(3), B(5), B(8), B(9) are very nearly parallel.

The platinum atom Pt(2) is directly bound to two dimethylphenylphosphine ligands with the Pt(2)–P(3) and Pt(2)–P(4) bond lengths of 234.1(4) pm and 232.4(4) pm respectively being

Table 2. Selected interatomic angles (°) for $[(PMe_2Ph)_4Pt_3B_{14}H_{16}]$ (**1**) with e.s.d.s in parentheses

(a) At Pt(2)			
P(3)–Pt(2)–P(4)	97.6(0.2)		
P(3)–Pt(2)–B(1)	97.9(0.5)	P(4)–Pt(2)–B(1)	134.8(0.5)
P(3)–Pt(2)–B(3)	85.3(0.4)	P(4)–Pt(2)–B(3)	174.8(0.5)
P(3)–Pt(2)–B(6)	143.7(0.4)	P(4)–Pt(2)–B(6)	97.9(0.4)
P(3)–Pt(2)–B(11)	158.3(0.5)	P(4)–Pt(2)–B(11)	97.5(0.5)
P(3)–Pt(2)–Pt(7)	113.4(0.1)	P(4)–Pt(2)–Pt(7)	123.8(0.1)
(b) At Pt(7)			
P(2)–Pt(7)–B(3)	49.0(0.4)	P(2)–Pt(7)–Pt(2)	132.6(0.1)
P(2)–Pt(7)–B(8)	90.2(0.5)	P(2)–Pt(7)–Pt(10)	146.3(0.1)
P(2)–Pt(7)–B(11)	175.5(0.5)	Pt(2)–Pt(7)–Pt(10)	76.0(0.0)
Pt(2)–Pt(7)–B(2′)	128.1(0.4)		
P(2)–Pt(7)–B(5′)	91.2(0.5)	B(11)–Pt(7)–B(3)	78.3(0.6)
		B(11)–Pt(7)–B(8)	94.3(0.6)
		B(11)–Pt(7)–B(2′)	47.9(0.6)
		B(11)–Pt(7)–B(5′)	86.4(0.6)
(c) At Pt(10)			
P(1)–Pt(10)–B(6)	133.1(0.4)	P(1)–Pt(10)–B(11)	172.3(0.5)
P(1)–Pt(10)–B(5)	100.4(0.5)	P(1)–Pt(10)–B(3′)	123.6(0.4)
P(1)–Pt(10)–B(9)	91.1(0.4)	P(1)–Pt(10)–B(9′)	89.6(0.4)
P(1)–Pt(10)–Pt(7)	146.3(0.1)		
B(11)–Pt(10)–B(9)	96.4(0.6)	B(11)–Pt(10)–B(9′)	84.5(0.6)
		B(9′)–Pt(10)–B(9)	128.9(0.6)
(d) At B(11)			
Pt(2)–B(11)–Pt(10)	132.5(0.8)		
Pt(1)–B(11)–Pt(10)	105.2(0.7)		
Pt(2)–B(11)–Pt(7)	88.6(0.6)		
B(6)–B(11)–Pt(2)	67.8(0.8)	B(6)–B(11)–B(2′)	157.7(1.3)
B(6)–B(11)–Pt(7)	129.8(1.1)	B(6)–B(11)–B(3′)	107.6(1.1)
B(6)–B(11)–Pt(10)	68.8(0.8)		
(e) At B(6)			
Pt(2)–B(6)–Pt(10)	123.1(0.7)	Pt(2)–B(6)–B(11)	64.1(0.7)
B(11)–B(6)–B(1)	104.3(1.1)	Pt(2)–B(6)–B(1)	64.9(0.7)
B(11)–B(6)–B(5)	109.5(1.2)	Pt(2)–B(6)–B(5)	117.6(1.0)
Pt(10)–B(6)–B(11)	62.2(0.7)		
Pt(10)–B(6)–B(1)	112.5(1.0)		
Pt(10)–B(6)–B(5)	66.6(0.8)		

similar to those observed in *nido*-platinaundecaborane clusters where the $Pt(PMe_2Ph)_2$ fragment is also bound to four boron atoms.[30,39–42] The platinum–boron distances for Pt(2) [B(1) 223.3(17), B(6) 225.0(16), B(3) 230.8(18), B(11) 218.6(17)] are also close to those expected from related compounds.[16] The platinum bonding environments for the two other platinum atoms Pt(7) and Pt(10) are of more interest since each is directly bound to only one dimethylphenylphosphine ligand [Pt(7)–P(2) 231.0(4) and Pt(10)–P(1) 228.8(4) pm] at normal platinum–phosphorus bond distances. The platinum atom Pt(7) is also directly bound to five boron atoms [B(3), B(8), B(11), B(2′), and B(5′)] and all are at typical bonding distances except for B(11) at a distance of 212.6(17) pm which is significantly shorter than the others. In fact this, together with the corresponding distance Pt(10)–B(11), is amongst the shortest platinum–boron distances yet reported in polyhedral metallaborane species, the only shorter one being 212(1) pm in $[(PMe_2Ph)_2Pt\text{-}\sigma,\eta^2\text{-}anti\text{-}B_{18}H_{20}]$.[42] Note also that the boron atom B(11) is nearly *trans* to P(2), with an angle B(11)–Pt(7)–P(2) of 175.5(0.5)°. The platinum atom Pt(10) is directly bound to six boron atoms [B(5), B(6), B(9), B(11), B(3′), and B(9′)] and once again all are

Table 3. Selected bond lengths (pm) for $[(PMe_2Ph)PtB_{16}H_{18}(PMe_2Ph)]$ (**2**) with e.s.d.s in parentheses

(a) From the platinum atom			
Pt(7)–P(1)	232.2(4)		
Pt(7)–B(2)	223.9(8)	Pt(7)–B(2′)	223.7(11)
Pt(7)–B(6)	227.4(11)	Pt(7)–B(6′)	224.7(20)
Pt(7)–B(8)	223.0(12)	Pt(7)–B(11′)	229.4(11)
(b) Boron–boron			
B(1)–B(2)	179.4(13)	B(1′)–B(2′)	178.4(15)
B(1)–B(3)	177.8(16)	B(1′)–B(3′)	179.7(14)
B(1)–B(4)	174.0(16)	B(1′)–B(4′)	180.0(15)
B(1)–B(5)	176.8(16)	B(1′)–B(5′)	176.0(15)
B(1)–B(6)	180.5(14)	B(1′)–B(6′)	177.1(22)
B(2)–B(3)	173.6(20)	B(2′)–B(3′)	175.0(15)
B(2)–B(6)	178.8(19)	B(2′)–B(6′)	187.2(24)
B(2)–B(8)	178.1(23)	B(3′)–B(4′)	180.2(14)
B(3)–B(4)	178.7(16)	B(3′)–B(9′)	178.4(15)
B(3)–B(8)	190.7(15)	B(4′)–B(5′)	178.5(16)
B(4)–B(5)	178.1(18)	B(4′)–B(9′)	175.1(15)
B(5)–B(6)	179.3(16)	B(4′)–B(10′)	177.4(16)
B(8)–B(2′)	182.4(14)	B(5′)–B(6′)	174.4(22)
B(8)–B(3′)	175.2(16)	B(5′)–B(10′)	180.1(15)
B(8)–B(9′)	163.1(15)	B(5′)–B(11′)	174.8(16)
		B(6′)–B(11′)	178.7(21)
		B(9′)–B(10′)	187.0(14)
		B(10′)–B(11′)	184.3(15)
(c) Other			
B(9′)–P(2)	191.8(11)		

Table 4. Selected interatomic angles (°) for $[(PMe_2Ph)PtB_{16}H_{18}(PMe_2Ph)]$ (**2**) with e.s.d.s in parentheses

(a) At the platinum atom			
P(1)–Pt(7)–B(2)	127.2(0.6)	P(1)–Pt(7)–B(2′)	138.3(0.3)
P(1)–Pt(7)–B(6)	88.3(0.3)	P(1)–Pt(7)–B(6′)	101.6(0.4)
P(1)–Pt(7)–B(8)	173.4(0.3)	P(1)–Pt(7)–B(11′)	92.3(0.3)
B(2)–Pt(7)–B(6)	46.7(0.5)	B(6)–Pt(7)–B(2′)	107.7(0.4)
B(2)–Pt(7)–B(2′)	88.4(0.6)	B(6)–Pt(7)–B(6′)	153.2(0.6)
B(2)–Pt(7)–B(6′)	131.1(0.7)	B(6)–Pt(7)–B(8)	87.8(0.4)
B(2)–Pt(7)–B(8)	47.0(0.6)	B(6)–Pt(7)–B(11′)	159.3(0.4)
B(2)–Pt(7)–B(11′)	120.2(0.4)	B(2′)–Pt(7)–B(6′)	49.3(0.6)
B(8)–Pt(7)–B(2′)	48.2(0.4)	B(2′)–Pt(7)–B(11′)	85.3(0.4)
B(8)–Pt(7)–B(6′)	84.1(0.6)	B(6′)–Pt(7)–B(11′)	46.3(0.5)
B(8)–Pt(7)–B(11′)	89.4(0.4)		
(b) Boron–boron–platinum			
B(1)–B(2)–Pt(7)	120.6(0.6)	B(8)–B(2′)–Pt(7)	65.7(0.5)
B(3)–B(2)–Pt(7)	116.5(0.8)	B(1′)–B(2′)–Pt(7)	116.5(0.6)
B(6)–B(2)–Pt(7)	67.7(0.5)	B(3′)–B(2′)–Pt(7)	118.0(0.6)
B(8)–B(2)–Pt(7)	66.2(0.5)	B(6′)–B(2′)–Pt(7)	65.6(0.7)
B(1)–B(6)–Pt(7)	118.3(0.6)	B(1′)–B(6′)–Pt(7)	116.5(1.1)
B(2)–B(6)–Pt(7)	65.7(0.5)	B(2′)–B(6′)–Pt(7)	65.0(0.7)
B(5)–B(6)–Pt(7)	118.8(0.7)	B(3′)–B(6′)–Pt(7)	116.8(1.0)
B(2)–B(8)–Pt(7)	66.8(0.5)	B(11′)–B(6′)–Pt(7)	68.2(0.7)
B(3)–B(8)–Pt(7)	109.9(0.7)	B(5′)–B(11′)–Pt(7)	114.4(0.7)
B(2′)–B(8)–Pt(7)	66.1(0.5)	B(6′)–B(11′)–Pt(7)	65.4(0.7)
B(3′)–B(8)–Pt(7)	118.3(0.6)	B(10′)–B(11′)–Pt(7)	107.2(0.6)
B(9′)–B(8)–Pt(7)	116.0(0.7)		
(c) Boron–boron–phosphorus			
B(8)–B(9′)–P(2)	123.5(0.7)	B(4′)–B(9′)–P(2)	116.3(0.7)
B(3′)–B(9′)–P(2)	120.1(0.7)	B(10′)–B(9′)–P(2)	117.7(0.6)

within normal bonding distances apart from B(11), which, as just mentioned, has a very short bonding distance of 212.3(16) pm and is approximately *trans* to the co-ordinated phosphorus atom P(1), the angle B(11)–Pt(10)–P(1) being 172.3(0.5)°. These

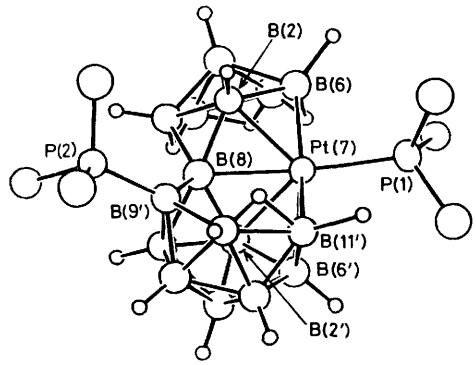

Figure 6. Molecular structure of the red 17-vertex monometallic compound $[(PMe_2Ph)PtB_{16}H_{18}(PMe_2Ph)]$ (**2**), with selected organophosphine component atoms omitted for clarity

interesting modes of co-ordination of the borane cluster to the platinum atoms Pt(7) and Pt(10) are discussed in more detail in section (*e*).

Hydrogen atoms were not located in the structure determination but selective ^1H-$\{^{11}B\}$ n.m.r. experiments [see section (*d*), Table 8] suggest that each boron atom except B(11) has a terminal hydrogen atom associated with it and that there are bridging boron–hydrogen–boron hydrogen atoms associated with B(5′)B(4′) and B(4′)B(9′). A third bridging hydrogen atom, presumably associated with the Pt(7)B(8)B(9)Pt(10) subface, has not been confirmed by n.m.r. spectroscopy but is inferred from the non-paramagnetic nature of the compound. Difficulty in precisely locating hydrogen atoms associated with diplatinum polyhedral boron-containing compounds has also been noted by other workers.[29,43]

(*c*) *Molecular Structure of* $[(PMe_2Ph)PtB_{16}H_{18}(PMe_2Ph)]$ (**2**).—An ORTEP plot of the macropolyhedral cluster compound $[7\text{-}(PMe_2Ph)\text{-}7\text{-}PtB_{16}H_{18}\text{-}9'\text{-}(PMe_2Ph)]$ (**2**) is shown in Figure 6. Selected interatomic distances and angles are in Tables 3 and 4 respectively. The heavy-atom structure consists of two open subclusters fused across their open faces and with Pt(7)B(8) as a common edge [see also Figure 5(*b*)]. The larger subcluster can be viewed as a *nido* 11-vertex PtB_{10} structure with a geometry based on an icosahedron with one vertex removed and it seems closely related to the well known *nido*-7-platinaundecaborane cluster compounds.[30,39–42] The smaller eight-vertex PtB_7 subcluster appears to have the same gross structure of both the *nido* and *arachno* eight-vertex binary borane species B_8H_{12} and B_8H_{14} and is based on a contiguous eight-vertex icosahedral fragment.

All terminal B–H and bridging B–H–B hydrogen atoms in the cluster were located and interatomic angles and distances are within the typical ranges[16,37,38] found in binary borane and metallaborane clusters. Two boron atoms in the cluster, B(8) and B(9′), are not directly bound to terminal or bridging hydrogen atoms. The boron atom B(8) is at the shared common edge of the two subclusters whilst B(9′) has its otherwise expected terminal hydrogen atom replaced by a dimethylphenylphosphine ligand group. This phosphorus–boron bond length, B(9′)–P(2), of 191.8(11) pm is consistent with a bond order of one and is typical for a phosphorus atom bound *exo* to a borane cage system.[16,18,21,44,45] With the exception of the distance B(8)–B(9′), all boron–boron distances and associated interatomic angles in both of the two subclusters are within the limits[37,38] expected for icosahedral fragments. The interboron distance for B(8)–B(9′) of 163.1(15) pm is rather short and presumably results from the 'extra electron' that B(9′) has

Table 5. Proton and phosphorus-31 n.m.r. data for the PMe_2Ph moieties in $[(PMe_2Ph)PtB_{16}H_{18}(PMe_2Ph)]$ (**2**), in $CDCl_3$ solution at +21 °C

	B-bound PMe_2Ph	Pt-bound PMe_2Ph
$\delta(^{31}P)$/p.p.m.[a]	−4.4	−2.4[b]
$^1J(^{195}Pt\text{–}^{31}P)$/Hz		2 891 ± 10[b]
$^1J(^{31}P\text{–}^{11}B)$/Hz	130 ± 30[c]	
$\delta(^1H)$/p.p.m.[d,e]	+1.99(A), +1.96(B)	+2.08(C), +2.00(D)
$^2J(^{31}P\text{–}^1H)$/Hz[d,f]	8.3(A), 8.5(B)	10.1(C), 9.8(D)
$^3J(^{195}Pt\text{–}^1H)$/Hz[d,f]		27.1(C), 26.8(D)

[a] ±0.2 p.p.m. to high field (low frequency) of 85% H_3PO_4. [b] At −50 °C in CD_2Cl_2 solution, $\delta(^{31}P)$ −1.6 p.p.m., $^1J(^{195}Pt\text{–}^{31}P)$ 2 883 ± 10 Hz. [c] Partially collapsed 1:1:1:1 quartet at +21 °C; at −50 °C the resonance was a hump with no resolved components. [d] A,B,C,D serve only to distinguish the four equivalent P-methyl groups. [e] ±0.02 p.p.m. to high field (low frequency) of $SiMe_4$. [f] ±0.03 Hz.

Table 6. Proton and boron-11 n.m.r. data for the metallaborane cluster atoms in $[(PMe_2Ph)PtB_{16}H_{18}(PMe_2Ph)]$ (**2**)

Tentative assignment	$\delta(^{11}B)$/p.p.m.[a] ($CD_3C_6D_5$, +110 °C)	$\delta(^{11}B)$/p.p.m.[a] ($CDCl_3$, +21 °C)	$\delta(^1H)$/p.p.m. (CD_2Cl_2, +22 °C)[b] *exo*-Terminal	Bridge
(*i*) B_6 subcluster				
2	+22.8[c]	+22.5[c]	+5.09[c]	
3[d]	+13.7	+13.0	+3.48	+0.60
4[d]	+13.1	*ca.* +12.5	+3.26	−0.65
5[d]	*ca.* +10	*ca.* +9.5	+3.76	−1.43
6[d]	+8.4	*ca.* +7.5	+3.47 or +3.11[e]	
1	−46.5	−47.5	−0.25	
(*ii*) PtB_{10} subcluster				
2′	+32.1[f]	+29.4[f]	+2.83	
8	+16.4[g]	+16.2	*h*	
4′[d]	+12.3	+10.6	+3.31	
6′[d]	+10.6	+8.6	+3.47 or +3.11[e]	
11′[d]	*ca.* +11	*ca.* +8	+2.97	
1′	−2.6	−4.9	+2.14[i]	
9′	−4.1	−4.0	*j*	
10′	−12.7	−13.9	+1.77	−0.34[k]
3′	−21.7	−22.9	+1.58	
5′	−23.2	−24.9	+1.87[l]	

[a] ±0.2 p.p.m. to high field (low frequency) of $BF_3(OEt_2)$ in $CDCl_3$ solution. [b] ±0.03 p.p.m. to high field (low frequency) of $SiMe_4$; proton resonances related to corresponding boron resonances by selected ^1H-$\{^{11}B\}$ spectroscopy; all measurable $^1J(^{11}B\text{–}^1H)$ values were in the range *ca.* 140—160 Hz. [c] $^1J(^{195}Pt\text{–}^{11}B)$ *ca.* 270 Hz, ^2J ($^{195}Pt\text{–}B\text{–}^1H$) *ca.* 44 Hz; signs opposite by selective ^1H-$\{^{11}B\}$ spectroscopy (ref. 51). [d] There are uncertainties in this region due to the mutually overlapping boron resonances; any satellite structure in this region arising from $^1J(^{195}Pt\text{–}^{11}B)$ [expected for B(6), B(6′), and B(11′)] is obscured. [e] Assignment ambiguous among $\delta(^{11}B)$ +7.5 and +8.6, ^1H-$\{^{11}B$(selective)$\}$ experiments inconclusive. [f] $^1J(^{195}Pt\text{–}^{11}B)$ *ca.* 220 Hz. [g] Possible $^1J(^{195}Pt\text{–}^{11}B)$ *ca.* 280 Hz. [h] Non-hydrogen bound *conjuncto* site. [i] $^3J(^{195}Pt\text{–}^1H)$ *ca.* 62 Hz. [j] PMe_2Ph-bound site; $^1J(^{31}P\text{–}^{11}B)$ *ca.* 130 Hz. [k] $^2J(^{195}Pt\text{–}^1H)$ *ca.* 55 Hz. [l] $^1J(^{195}Pt\text{–}^1H)$ *ca.* 45 Hz.

available for cluster bonding (brought about by the two-electron *exo*-phosphine ligand) being somewhat localized in a B(8)–B(9′) bonding orbital. The platinum–phosphorus bond length Pt(7)–P(1) of 232.2(4) pm and platinum–boron distances of 229.4(11) to B(11′), 224.7(20) to B(6′), 223.7(11) to B(2′), 223.0(12) to B(8), 223.9(8) to B(2), and 227.4(11) to B(6), are unexceptional when compared to other known platinaborane

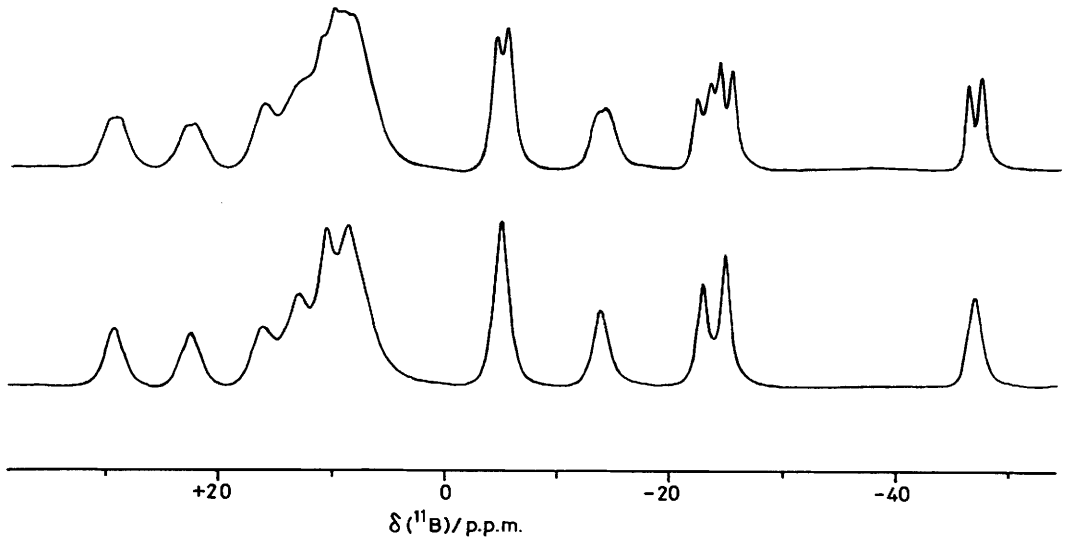

Figure 7. 128-MHz ^{11}B n.m.r. spectra of $[(PMe_2Ph)PtB_{16}H_{18}(PMe_2Ph)]$ (**2**) in $CDCl_3$ solution at +25 °C. The upper trace shows the normal spectrum, and the lower trace a spectrum with ^1H(broad-band noise) decoupling. A broad baseline hump, arising from ^{11}B signals associated with boron in ceramic materials used in the n.m.r. probe construction, has been eliminated by baseline-subtraction procedures

cluster compounds.[16,27,29,30,39–42,46,47] The 'zigzag' arrangement of the hexahapto borane ligand around the platinum atom [see Figure 14(*a*)] is of more interest and is discussed in greater detail in section (*e*).

(*d*) *Nuclear Magnetic Resonance Investigations.*—It is convenient to discuss $[(PMe_2Ph)PtB_{16}H_{18}(PMe_2Ph)]$ (**2**) first. Details of the ^{31}P, ^{11}B, and ^1H coupling constants and chemical shifts are given in Tables 5 and 6, and the 128-MHz ^{11}B spectrum is in Figure 7. The n.m.r. parameters are consistent with the single-crystal molecular structure [section (*c*) above, Figure 6], thus confirming that the crystal chosen was representative of the bulk sample. Thus two phosphorus environments are apparent (Table 5), one exhibiting $^1J(^{31}P-^{11}B)$ coupling of a magnitude consistent with an exo-polyhedral direct two-electron two-centre phosphorus–boron bond,[15,18,21,48] and one exhibiting $^1J(^{195}Pt-^{31}P)$ coupling of a magnitude typical for a platinum-bound PMe_2Ph ligand *trans* to multicentre platinum-to-borane bonding.[16,27–30,36,39,48,49] The phosphorus chemical shifts are also typical for these two environments, and the two inequivalent methyl groups of each of these two phosphines are readily apparent in the proton spectrum (Table 5).

The 16 different ^{11}B resonance positions expected for (**2**) can be distinguished by integrated ^{11}B and $^{11}B-\{^1H$(broad-band noise)$\}$ spectroscopy, with most of the overlap ambiguities being resolved by ^1H spectroscopy using selective ^{11}B irradiation.[50,51] This last technique enabled the effective resolution in the ^{11}B spectrum to be increased in the region $\delta(^{11}B)$ +7 to +15 p.p.m. ($CDCl_3$ solution), which contains seven overlapping peaks, and also permitted the assignment of the 14 *exo*-terminal proton resonances to their directly-bound boron atoms. Some minor *exo*-proton–boron-11 correlation ambiguities remain in the overlap region associated with $\delta(^{11}B)$ +9 to +15 p.p.m., but differentiation of these is not at present crucial because this ^{11}B shift range is narrow and because there are no anomalous proton shieldings in this region. It may be noted that the observed differential solvent effects on boron nuclear shielding of up to 2 p.p.m. or so in this overlap area produce marked changes in the curve shape of the seven-resonance agglomerate in this part of the spectrum as the solvent is varied. In addition to the seven *exo*-terminal

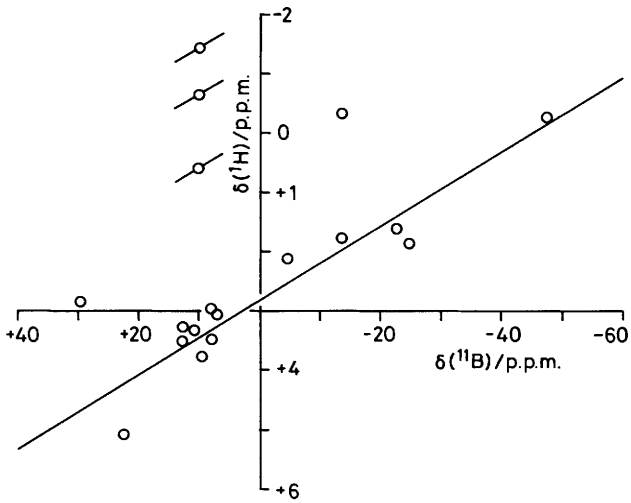

Figure 8. Proton–boron-11 nuclear shielding correlation plot for $[(PMe_2Ph)PtB_{16}H_{18}(PMe_2Ph)]$ (**2**) (CD_2Cl_2 solution). The line drawn represents a gradient $\delta(^{11}B):\delta(^1H)$ of 16:1

hydrogen atoms, this seven-resonance overlap area of $\delta(^{11}B)$ +9 to +15 p.p.m. in the boron-11 spectrum is also associated with three bridging hydrogen atoms. A fourth proton resonance in the bridging region, at $\delta(^1H)$ −0.34 p.p.m., was associated specifically in the $^1H-\{^{11}B\}$ experiments only with one boron resonance at $\delta(^{11}B)$ −13.9 p.p.m. ($CDCl_3$ solution), rather than with two different boron sites expected for a bridging hydrogen atom. The proton is probably that in the (10′)(11′) bridging position (see assignments below), and it is of interest that the coupling $^1J[^{11}B(10')-^1H$(bridge)] is so small in this case, even though a typical coupling $^2J[^{195}Pt-B(10')-^1H$(bridge)] of *ca.* 55 Hz is retained.

A proton–boron-11 shielding correlation plot is given in Figure 8. It can be seen that most of the *exo*-terminal protons lie close to a line of gradient $\delta(^{11}B):\delta(^1H)$ 16:1 as found for a variety of other platinaboranes and related compounds,[27–30,40,44,48,50,51] with the bridging protons some 2—6

p.p.m. above the plot as expected. Only two *exo*-proton data deviate significantly from this generalization, *viz.* those associated with the two least shielded boron resonances at $\delta(^{11}B)$ +22.5 and +29.4 p.p.m. ($CDCl_3$ solution). These are probably at positions adjacent to the platinum centre [at B(2) and B(2′) respectively; see following paragraph]; as such, each is held in a position close over the open face of an opposing subcluster and might therefore be expected to show anomalous shielding behaviour, perhaps arising from the magnetic anisotropy of the metal centre and/or the cluster open faces.

By comparison with data for known compounds such as $[(PMe_2Ph)_2Pt_2B_{12}H_{18}]$[28] and $[(PMe_2Ph)_2PtB_{10}H_{12}]$[51] [in which the intracluster bonding will have parallels with that in the subclusters of (2)], and from the results of COSY two-dimensional n.m.r. spectroscopy, a tentative assignment of most of the resonance positions (as indicated in Table 6) can be made. The extreme high-field ^{11}B resonance is reasonably ascribed to the apical boron atom B(1) in the B_6H_9 subcluster, and the two next highest field resonances [around $\delta(^{11}B)$ −24 p.p.m.] to the apical B(3′) and B(5′) positions in the PtB_{10} subcluster. The platinum-coupled resonance at $\delta(^{11}B)$ +16.2 p.p.m. ($CDCl_3$ solution), which has no *exo*-terminal proton associated with it, is readily assigned to the *conjuncto* position B(8), and that at −4.0 p.p.m. ($CDCl_3$ solution), which exhibits coupling $^1J(^{31}P-^{11}B)$, to the phosphine-bound boron atom B(9′). In addition, the two extreme low-field resonances exhibit couplings $^nJ(^{195}Pt-^{11}B)$ of a magnitude consistent with $n = 1$,[27,48,51] which assigns them to platinum-bound positions. This information together with the results of 'two-dimensional' homonuclear boron-11–boron-11 correlation n.m.r. spectroscopy (two-dimensional COSY n.m.r.) (Figure 9) then permits the assignments indicated in Table 5, for which further support arises from the incidence of the couplings $^nJ(^{195}Pt-^1H)$ (where $n = 2$ or 3) that are observable for $^1H(2)$, $^1H(1')$, $^1H(5')$, and $^1H(10')(11')$(bridge), and which are consistent with known coupling paths in this type of system.[27–30,51]

Aspects of the results from the $^{11}B-^{11}B$ COSY n.m.r. experiments merit further brief comment. Polyhedral borane species have one-bond* interboron coupling constants $^1J(^{11}B-^{11}B)$ of up to one or two tens of Hz, with longer range couplings usually being effectively zero,[48] and therefore ^{11}B homonuclear correlation experiments which rely on these couplings offer a means of establishing the interboron connectivity throughout the cluster. This then readily permits an assignment of boron resonances to specific boron atoms in known structures, long a problem in the development of polyhedral borane n.m.r. spectroscopy, and also in principle permits the establishment of gross cluster geometry without having to resort to single-crystal *X*-ray diffraction techniques. These correlations were first explored over a decade ago in some elegant work using homonuclear continuous-wave INDOR $^{11}B-\{^{11}B\}$ spectroscopy,[52–56] but they can now be established conveniently on commercially available multiple-pulse Fourier-transform equipment with the aid of pulse sequences such as the Jeener-type[57] COSY one used here.[32,48,58–60] Some general considerations on the application of this technique to polyhedral borane species have recently been reviewed.[61]

It is emphasized that the observation of a correlation using these techniques is critically dependent on the magnitude of the internuclear spin–spin coupling.[48] Thus, for example, if the ^{11}B relaxation rate excessively exceeds the coupling constant, then no correlation will be seen. Also, if the coupling constant is effectively zero, even though a strong bond may exist, then similarly no correlation will be observed. This latter commonly happens, for example, in two-electron three-centre B–H–B bridging bonds and also in the 'long' interboron distances such as those in the B(5)–B(10)/B(7)–B(8) linkages in *nido*-decaboranyl clusters,[52–56] although exceptions to both these generalizations are known.[62–64] It is also known to occur in other specific instances, for example between the strongly bound adjacent B(1) and B(3) atoms in the *closo*-carborane 2,4-$C_2B_5H_7$.[58] Conversely, if longer range interboron spin–spin couplings happen to be large, then correlations can in principle be observable between non-adjacent boron centres, particularly so if the ^{11}B relaxation times are long.[48]

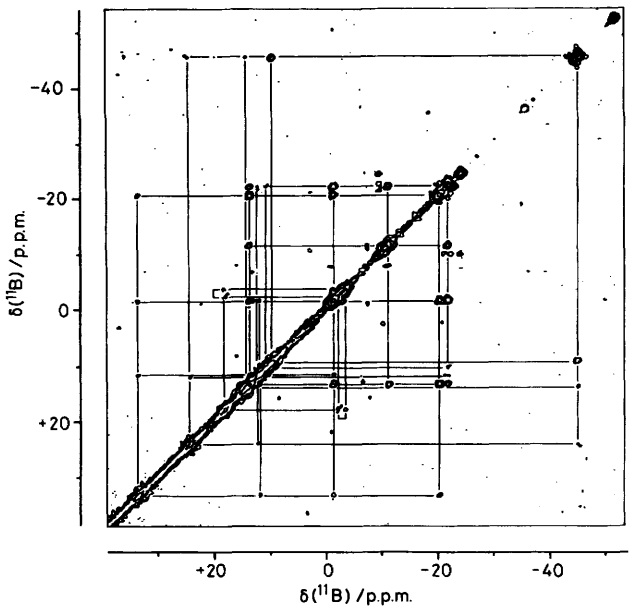

Figure 9. Symmetrized 128-MHz homonuclear ^{11}B two-dimensional COSY-45 contour plot for $[(PMe_2Ph)PtB_{16}H_{18}(PMe_2Ph)]$ (2), recorded for a saturated solution in $CD_3C_6D_5$ at +110 °C under conditions of continuous ^1H(broad-band noise) decoupling. Note there are small differences in $\delta(^{11}B)$ between this solution and a solution in $CDCl_3$ at ambient temperature (Table 6)

Some of these effects are apparent in the two-dimensional correlation work reported here (Figure 9). The macropolyhedral species $[(PMe_2Ph)PtB_{16}H_{18}(PMe_2Ph)]$ (2) is a large molecule, and at ambient temperature most of the ^{11}B resonances were too broadened by relaxation to show strong mutual correlations. This problem was partly overcome by conducting the experiments at higher temperatures, under which conditions the ^{11}B relaxation times are longer and their linewidths correspondingly narrower, but even so not all the expected correlations were observable and during the course of the experiment (overnight, +110 °C, $CD_3C_6D_5$ solution) some 20% decomposition occurred. The correlation plot therefore also shows peaks due to decomposition products. Any off-diagonal peaks arising from these do not correlate with peaks due to compound (2), however, and so can be readily eliminated from the analysis.

At this higher temperature (Figure 9) there is strong correlation among the apical boron nuclei in the 1′, 3′, 4′, and 5′ positions in the PtB_{10} subcluster. In general there is sufficient correlation between at least two of these and each of the nuclei in the 2′, 6′, 9′, and 10′ positions to establish their assignments with little ambiguity when considered in conjunction with the other evidence summarized above. Of the other two positions in

* Note that, in polyhedral chemistry, the superscript *n* in the descriptor ^nJ signifies the number of polyhedral edges on the shortest edge-path connecting the two nuclei in question, and, in contrast to classical structures, does *not* generally imply a coupling pathway defined by *n* two-electron two-centre bonds.

the PtB_{10} subcluster, the *conjuncto* $^{11}B(8)$ resonance is readily assigned because it lacks an *exo*-terminal proton, and the broad peak at $\delta(^{11}B)$ *ca.* +8 ($CDCl_3$ solution) will correspond to B(11) because of its (albeit weak) correlation with $^{11}B(5')$. The overall shielding pattern thus established for this PtB_{10} subcluster is similar to those observed in a variety of substituted *nido*-7-platinaundecaborane species.[30,40,51,65] This indicates a general similarity of electronic structure [see section (*e*)], the exception to this generalization being the low-field $^{11}B(2')$ resonance which is somewhat less shielded than usually found for a *nido*-7-platinaundecaboranyl system, and which, interestingly, also exhibits anomalies in the proton–boron-11 shielding correlation plot in Figure 8 above. The $B_{10}H_{12}$ fragments of *nido*-7-platinaboranes exhibit ten-vertex *nido*-decaboranyl bonding character on the periphery of their open face distant from the metal atom,[16] and consistent with this in compound (**2**) there is no correlation between the two boron nuclei joined by the B(10′)–H–B(11′) two-electron three-centre bond, or between the nuclei involved in the 'longer' B(9′)–B(10′) linkage. Interestingly in this context, $^{11}B(8)$–$^{11}B(9')$, which, in contrast to the corresponding position in *nido*-decaborane, is unbridged, does show a reasonable correlation.

Within the B_6 subcluster the apical boron resonance $^{11}B(1)$ at δ −47.5 p.p.m. ($CDCl_3$ solution) shows a stronger correlation with one resonance, and weaker ones with two others. These three, plus the two remaining unassigned resonances, must therefore be associated with the 2, 3, 4, 5, and 6 positions. However, the lack of any mutual correlation among these latter five peaks and between any of them and the *conjuncto* $^{11}B(8)$ resonance precludes their assignment to specific positions, although the presence of coupling $^1J(^{195}Pt–^{11}B)$ to the peak at $\delta(^{11}B)$ +22.5 p.p.m. ($CDCl_3$, Table 6) must limit this to B(2) or B(3). All the other four exhibit mutually similar shieldings, and so their precise assignment is not critical at present. The overall shielding pattern in this B_6 subcluster very much resembles that of a basally-substituted *mono*-hexaboranyl species, which indicates a similar electronic configuration [Figure 12(*b*), section (*e*) below].

The n.m.r. data that we have been able to gather for $[(PMe_2Ph)_4Pt_3B_{14}H_{16}]$ (**1**), although less definitive than for (**2**), are also consistent with the crystal and molecular structures (Figures 3 and 4 above).

The ^{31}P spectrum exhibits four resonances in the region $\delta(^{31}P)$ +10 to −20 p.p.m., typical of platinum-bound PMe_2Ph moieties *trans* to platinum–borane linkages, and correspondingly eight inequivalent P-methyl doublets are apparent in the ^1H spectrum (Table 7). All four ^{31}P resonances have satellites arising from couplings $^1J(^{195}Pt–^{31}P)$. Two of these couplings, *ca.* 2 700 Hz, are typical for platinum-bound PMe_2Ph ligands *trans* to platinum–borane multicentre bonding (see refs. 16, 27–30, 48), but the other two of these couplings, at >3 000 Hz, are somewhat larger than those generally found previously, although larger couplings have occasionally been observed in particular platinacarborane clusters.[48] Two of the ^{31}P resonances also exhibit longer range coupling to ^{195}Pt, probably a geminal coupling $^2J(^{195}Pt–Pt–^{31}P)$ within the Pt(2)–Pt(7) system. All four ^{31}P resonances show inter-phosphorus couplings with magnitudes of between 4 and 27 Hz, which indicate coupling paths $^3J(^{31}P–Pt–Pt–^{31}P)$ and $^4J(^{31}P–Pt–B–Pt–^{31}P)$ as well as the expected $^2J(^{31}P–Pt–^{31}P)(cis)$. Longer range couplings such as these,

Table 7. Proton[a] and phosphorus-31[b] n.m.r. data for the PMe_2Ph ligands in $[(PMe_2Ph)_4Pt_3B_{14}H_{16}]$ (**1**)

$\delta(^{31}P)$/p.p.m.	$^1J(^{195}Pt–^{31}P)$/ Hz	$^nJ(^{195}Pt–^{31}P)$/ Hz	$^nJ(^{31}P–^{31}P)$/ Hz
+3.1	3 044	*c*	27
−2.4	2 652	55	27, 20
−5.0	2 783	*c*	4
−11.2	3 035	40	4.20

[a] P-Methyl doublets centred at $\delta(^1H)$ 2.13, 2.10, 2.01, 1.89, 1.80, 1.60, 1.40, and 1.25 p.p.m.; $CDCl_3$ solution at +21 °C; all exhibited coupling $^2J(^{31}P–^1H)$ of *ca.* 8—9 Hz and had satellites due to $^3J(^{195}Pt–^1H)$ of *ca.* 25—30 Hz; overlap precluded an exact measurement of these couplings. [b] In CD_2Cl_2 solution at −50 °C; $\delta(^{31}P)$ ±0.1 p.p.m. to high field (low frequency) of 85% H_3PO_4; coupling constants ±2 Hz. [c] Small or zero.

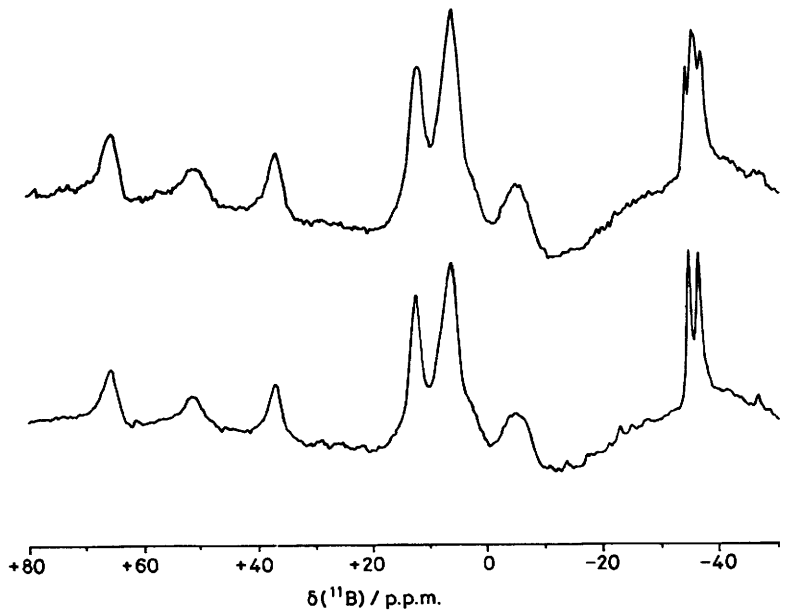

Figure 10. 128-MHz ^{11}B n.m.r. spectra of $[(PMe_2Ph)_4Pt_3B_{14}H_{16}]$ (**1**) in $CDCl_3$ solution at +25 °C. The upper trace shows the normal spectrum and the lower trace a spectrum with ^1H(broad-band noise) decoupling. Baseline subtraction procedures have been used to minimize the baseline hump mentioned in Figure 7

Table 8. Proton and boron-11 chemical shifts[a] for the metallaborane cluster atoms in $[(PMe_2Ph)_4Pt_3B_{14}H_{16}]$ (**1**), in CD_2Cl_2 solution at +21 °C

δ(¹¹B)/p.p.m.	δ(¹H)/p.p.m.	
+66.0[b]		
+57.4	+3.93	
+37.4	+5.42	
+13.2	+2.62	
ca. +13	+4.52	
ca. +8	*ca.* +3.6	
ca. +7	*ca.* +3.8	
+6.8	+3.75	
ca. +5	*ca.* +3.7	
ca. +2	+3.80	−1.59[c], −1.95[c]
ca. −3	+2.20	
ca. −6	+2.33[d]	
−34.1[e]	+0.42	
−36.1[e]	+0.81	

[a] To high field (low frequency) of $SiMe_4$ and $BF_3(OEt_2)$ in $CDCl_3$ respectively. [b] *Conjuncto* position B(11). [c] ^1H Resonances assigned to corresponding ^{11}B resonances by selective ^1H-{^{11}B} spectroscopy; there is uncertainty in the precise assignments and chemical shift values in the region δ(^{11}B) +13 to −6 p.p.m. and δ(^1H) +2.2 to +3.8 p.p.m. [d] Possible doublet of doublets, splittings *ca.* 20 and 60 Hz. [e] Probably apical positions B(1) and B(1′).

involving ^{195}Pt and/or ^{31}P through polyhedral metallaborane systems, are becoming increasingly well documented.[18,27,28,36,48] Assignment of the phosphorus resonances among P(1), P(2), P(3), and P(4) is not at present possible, although it is likely that the resonance exhibiting the weakest interphosphorus coupling is that due to P(1) on the more isolated Pt(10) position.

The analysis of the ^{11}B spectra of compound (**1**) (Figure 10 and Table 8) is more difficult than for (**2**) as the lines are generally somewhat broader than those for the latter species. This is because of the greater molecular extent and bulk of compound (**1**) [113 atoms *versus* 75 atoms for (**2**)] which inhibits its mobility in solution, thereby reducing the correlation time τ_c and inducing more rapid quadrupolar relaxation.[48] Although five individual resonances, at extreme high and low field, are readily apparent in the 128-MHz spectrum, the remaining nine overlapping resonances in the central region are difficult to resolve, even with the aid of the ^1H-{^{11}B} technique.[51] Consequently a number of the ^{11}B chemical shifts given in Table 8 are subject to some uncertainty. It is of interest that the overall ^{11}B shielding pattern has similarities to those of $[(PMe_2Ph)_2Pt_2B_{12}H_{18}]$ (**3**) and its asymmetrically substituted derivative $[(PMe_2Ph)_4HPt_3B_{12}H_{17}]$,[28] indicating that the bonding in the formally *nido*-hexaborane-like B_6 cluster fragments in these two species, and in the corresponding B(1,3,4,5,8,9) and B(1′,2′,3′,4′,5′,9′) units of compound (**1**), may well be quite similar [see also section (*e*) below, Figure 12].

Selective ^1H-{^{11}B} spectroscopy involving the five well separated extreme high- and low-field ^{11}B resonances was straightforward, and readily identified the *exo*-terminal ^1H resonances associated with four of these, and showed that the most extreme low-field ^{11}B resonance is not associated with a directly bound proton, and therefore presumably arises from the *conjuncto* boron atom B(11). The results of ^1H-{^{11}B(selective)} experiments were much less satisfactory in the central region of the spectrum because there is considerable overlap within the ^1H as well as the ^{11}B spectra, even at 400-MHz ^1H or 128-MHz ^{11}B field strengths. The results, however, were not inconsistent with there being a terminal proton associated with each of the nine remaining boron atoms, a conclusion consistent in turn

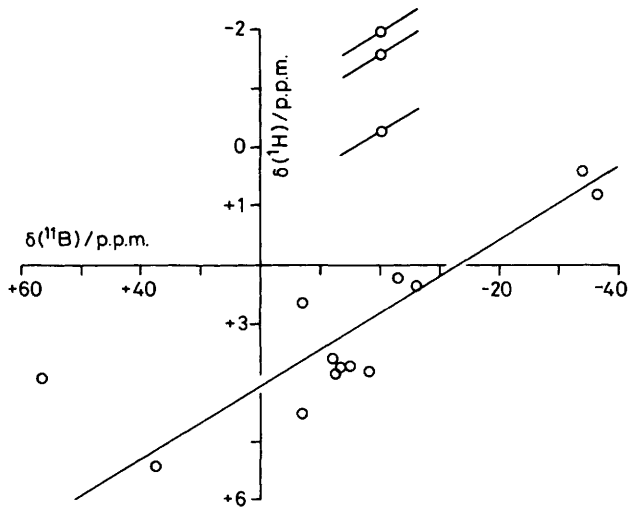

Figure 11. Proton–boron-11 nuclear shielding correlation plot for $[(PMe_2Ph)_4Pt_3B_{14}H_{16}]$ (**1**) (CD_2Cl_2 solution at +21 °C). The line drawn represents the gradient δ(^{11}B):δ(^1H) of 16:1

with the molecular geometry about each of these sites [section (*b*) above]. However, only two ^1H resonances, at δ(^1H) −1.59 and −1.95 p.p.m. [presumably those associated with B(4′)B(5′) and B(4′)B(9′)] were apparent in the region generally associated with bridging hydrogen atoms, whereas the diamagnetism of the compound requires an additional hydrogen atom to be associated with the molecule, presumably at the B(8)B(9) bridging position on the open face of the Pt_3B_8 subcluster [see section (*b*) above]. There was, however, no evidence for this in the expected high-field ^1H bridging region of the spectrum. The resonance could however be in the complex overlapping region at δ(^1H) +2 to +4 p.p.m. because there was sufficient ambiguity in the results of the selective ^1H-{^{11}B} experiments to allow for this. If this were the case, however, then the nuclear shielding would be anomalously low for a conventional bridging atom. This could be a consequence of the unique environment in the Pt_2B_3 open face of the Pt_3B_8 subcluster, although it should be pointed out that ostensibly similar disposed bridging protons in the M_2B_3 open face of *nido* 11-vertex species such as $[(o\text{-}PPh_3)(o\text{-}Ph_2PC_6H_4)HIrB_9H_{10}Pt(PMe_3)_2]$[41] do not show anomalously low shielding behaviour.[18] However, as mentioned above [section (*b*)], other workers have also had difficulty in pinpointing similar hydride types in this type of system.[43]

Apart from this, and as with compound (**2**), a proton–boron-11 shielding correlation plot for (**1**) shows little deviation from an approximately linear relationship δ(^{11}B):δ(^1H) = 16:1 (Figure 11). The exception again occurs at low field, in that the proton shielding associated with δ(^{11}B) +57.4 p.p.m. is some +2 to +3 p.p.m. greater than expected. In this it parallels the data for B(2) and B(2′) in compound (**2**) (Figure 8 above) and may therefore be associated with a similar environment in (**1**), perhaps the B(4′) position, although the low ^{11}B shielding would perhaps argue against this and favour ascription to B(6) instead [*cf.* δ(^{11}B) +59.7 for B(3) in (**3**)].[28]

(*e*) *Modes of Bonding of Platinum with the Borane Cluster.*—Macropolyhedral clusters are large polyhedral cluster compounds derived, albeit notionally rather than synthetically, from the fusion of two (or more) smaller polyhedral subclusters. Atoms common to both clusters can be described as being in '*conjuncto*' positions,[37] and in compounds (**1**), (**2**), and (**3**) it is of interest to note that (with one exception) all the platinum atoms are found at these *conjuncto* sites (Figure 5). This

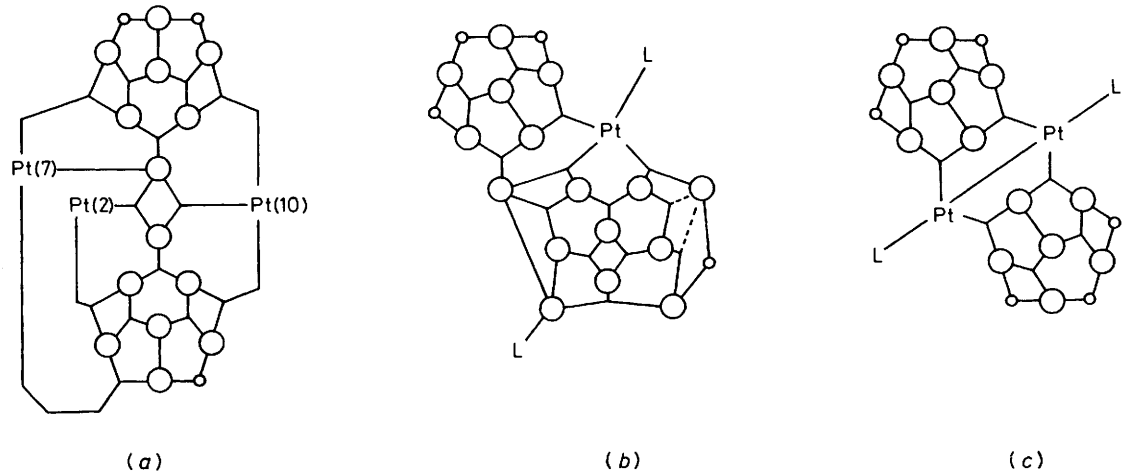

Figure 12. Simple valence-bond topological schemes for (*a*) $[(PMe_2Ph)_4Pt_3B_{14}H_{16}]$ (**1**), (*b*) $[(PMe_2Ph)PtB_{16}H_{18}(PMe_2Ph)]$ (**2**), and (*c*) $[(PMe_2Ph)_2Pt_2B_{12}H_{18}]$ (**3**)

positioning of the platinum atoms can be regarded as a reflection on the non-conical nature of the electrolobal* contribution to the cluster of these metal–phosphine fragments [structure (**V**)].

The structures of (**1**), (**2**), and (**3**) can be rationalized if, in the first instance, all the metal cluster vertices are considered to be square-planar 16-electron platinum(II) centres. Thus the neutral $Pt(PMe_2Ph)_2$ fragment in (**1**) can be considered to contribute two orbitals and two electrons to the cluster bonding σ framework, and each neutral $Pt(PMe_2Ph)$ fragment in (**1**), (**2**), and (**3**) three orbitals and two electrons. In both types of fragment the distribution of the bonding orbitals about the platinum centre approximates to a square-planar arrangement [see structures (**IV**) and (**V**)]. Accordingly, topological valence-bond descriptions for (**1**), (**2**), and (**3**) can be drawn in which all the platinum atoms are considered as 16-electron platinum(II) centres (see Figure 12).

Such a description is most easily seen for (**3**) which is composed of two eight-vertex Pt_2B_6 subclusters fused so as to have the two platinum atoms common to both [see Figures 2 and 5(*c*)]. In this model [Figure 12(*c*)], there is a direct platinum–platinum bond (264.4 pm, consistent with bond-order one), and there are two trihapto *nido*-B_6H_9 units, each bound to the pair of platinum atoms by two two-electron three-centre bonds.[28] This description, together with the observed geometry, is consistent with each platinum atom supplying three orbitals and two electrons to the cluster bonding framework within the context of an overall four-orbital square-planar metal bonding-orbital disposition. An essentially identical description of bonding about the cluster platinum atoms can be invoked for the smaller macropolyhedral cluster compound $[(PMe_2Ph)_2Pt_2B_8H_{14}]$ (Figure 13), which also contains a linear $PhMe_2P$–Pt–Pt–PMe_2Ph fragment, now co-ordinated by *nido*-B_6H_9 and *nido*-B_2H_5 fragments.[29,46]

$Pt(PMe_2Ph)$ fragments also occur in (**1**) and (**2**). Of these, the platinum atom Pt(7) in (**2**) is directly bound to six boron atoms B(2), B(6), B(8), B(2′), B(6′), and B(11′) and a view looking down the P(1)–Pt(7) bond is shown in Figure 14(*a*). A

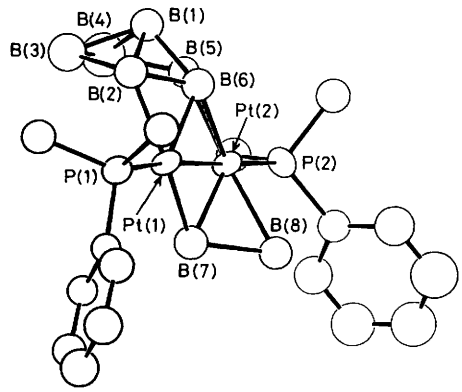

Figure 13. ORTEP drawing of the molecular structure of the yellow 10-vertex bimetallic species $[(PMe_2Ph)_2Pt_2B_8H_{14}]$.[29,46] Hydrogen atoms were not located in the diffraction analysis, but n.m.r. spectroscopy shows that each boron atom has an *exo*-terminal hydrogen bound to it, and suggests that there are bridging hydrogen atoms at cluster sites B(3)B(4), B(4)B(5), B(5)B(6), B(7)B(8), and Pt(1)B(7)[29]

topological valence-bond description of the cluster can be drawn as in Figure 12(*b*) and in this the metal atom forms three three-centre, two-electron bonds with the boron atom pairs B(6′)B(11′), B(2′)B(8), and B(2)B(6) and receives a co-ordinate donor bond from P(1). A similar bonding mode can be proposed for the $Pt(PMe_2Ph)$ fragment at Pt(10) in (**1**), in which the metal atom is also bound to six boron atoms and the borane ligand can be considered to co-ordinate in a tridentate manner [η^2-B(3′)B(9′), η^2-B(11)B(6), and η^2-B(5)B(9)] to the metal centre with the fourth platinum bonding orbital filled by a dimethylphenylphosphine donor pair [see Figure 12(*a*)]. The bonding of the platinum atoms in these cluster environments can be judged from Figure 14(*a*) and (*b*) to approximate to a distorted square plane. However, the shorter Pt(10)–B(11) internuclear distance in (**1**) implies some two-electron two-centre character, and this together with the position of B(11) relative to P(1) (being approximately *trans*) indicates that the above description is undoubtedly oversimplified [see discussion of bonding for (**3**) in ref. 28].

The other $Pt(PMe_2Ph)$ fragment in (**1**), *i.e.* that at Pt(7), is directly bound to five boron atoms [B(3), B(8), B(11), B(2′), and B(5′)]. A possible topological valence-bond description as

* We use the term 'electrolobal' to describe conveniently the combined electronic and orbital contributions that a (specified) fragment may make to a cluster bonding scheme. Thus, for example, in *closo*-$[B_{12}H_{12}]^{2-}$, the electrolobal contribution of a notional BH fragment would be three orbitals and two electrons, and that of a notional BH^- three orbitals and three electrons.

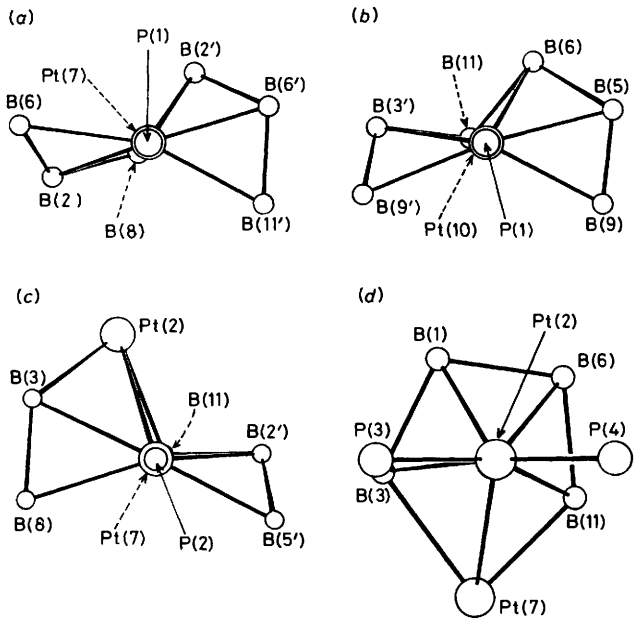

Figure 14. Views of the platinum and circumjacent atoms in green $[(PMe_2Ph)_4Pt_3B_{14}H_{16}]$ (**1**) and red $[(PMe_2Ph)PtB_{16}H_{18}(PMe_2Ph)]$ (**2**). (*a*) The hexahapto-co-ordinated Pt(7) atom in (**2**), viewed down the P(1)–Pt(7) vector; (*b*) the hexahapto-co-ordinated Pt(10) atom in (**1**), viewed down the P(1)–Pt(10) vector; (*c*) the hexa/heptahapto-co-ordinated Pt(7) atom in (**1**), viewed down the P(2)–Pt(7) vector; and (*d*) the hexa/heptahapto-co-ordinated Pt(2) atom in (**1**), viewed approximately down the bisector of the P(3)–Pt(2)–P(4) angle

shown in Figure 12(*a*) suggests that the tridentate borane ligand co-ordinates η^2-B(3)B(8), σ-B(11), and η^2-B(2')B(5') to the metal centre. In agreement with this the Pt(7)–B(11) interatomic distance is shorter than all the other Pt(7)–B distances and B(11) is approximately *trans* to P(2). However, again this appears oversimplified since Pt(2) is at a distance of only 301.2(1) pm from Pt(7) and this distance is too short to be completely non-bonding. A view of this metal centre looking down the P(2)–Pt(7) bond is shown in Figure 14(*c*). It is of interest to note that the position of Pt(2) relative to Pt(7) is essentially the same as the relative position of B(6) to Pt(10) also in (**1**) and of B(2') to Pt(7) in (**2**).

Finally, the $Pt(PMe_2Ph)_2$ fragment in (**1**), at Pt(2), can in the first instance be considered as contributing two orbitals and two electrons to the cluster bonding σ framework and a topological valence-bond scheme such as in Figure 12(*a*) can be drawn in which the metal forms two three-centre/two-electron bonds with the pairs of boron atoms B(3)B(1) and B(6)B(11). This interpretation, however, does not include any interaction between Pt(2) and Pt(7) and again appears to be over simplified. A view of this cluster vertex, looking approximately along the bisector of the angle P(3)–Pt(2)–P(4) into the cluster, is shown in Figure 14(*d*). It can be seen that the Pt(2) atom occupies a position directly above the centre of the pentagon of approximately coplanar atoms [B(3),B(1),B(6),B(11), and Pt(7)] to which it is directly connected. In this position the Pt(2) atom appears to be mimicking a boron atom and may well be contributing an additional orbital to the cluster bonding scheme by becoming a pseudo-conical fragment. The P(3)P(4)Pt(2)B(1)B(3)B(6)B(11) bonding geometry is very similar to that in *nido*-platinaundecaboranes such as $[(PMe_2Ph)_2PtB_{10}H_{12}]$,[39] implying significant contributions from valence-bond structures with three two-electron metal-to-borane bonds: two two-centre to B(3) and B(11), and one three-centre to B(1)B(6).[16] In this environment, the interaction between the two platinum atoms Pt(2) and Pt(7) can then be envisaged as a (weakish) dative two-electron bond from Pt(7) to Pt(2), with Pt(2) then tending towards an 18-electron configuration. This necessitates contributions from a four-orbital platinum(IV)-type interaction of Pt(7) with the other cluster atoms; the four Pt(7) cluster bonding orbitals would then be arranged as in Figure 15 with three orbitals in the square plane and one at *ca.* 45° to this plane in a position which would correspond to a capping position in a 'capped octahedral' environment. Similar contributions from higher metal valence states may also be significant in accounting for the observed distortions from square planar at the other platinum centres discussed above [Figure 14(*a*)—(*c*)], and they have also been used in descriptions of the bonding in the related species $[(PMe_2Ph)_2Pt_2B_8H_{14}]$(Figure 13)and$[(PMe_2Ph)_2Pt_2B_{12}H_{18}]$ (**3**) (Figure 2), as discussed in detail elsewhere.[28,29,46]

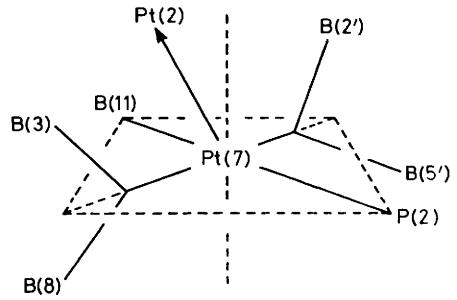

Figure 15. Proposed distribution of simple bonding vectors about the Pt(7) atom in (**1**). This consists of essentially square-planar co-ordination involving two-electron three-centre bonds [to B(2)B(5) and B(3)B(8)]; in addition weak dative two-electron two-centre bonding interaction to Pt(2) is proposed

We also note that, if the $Pt(PMe_2Ph)$ vertices in compounds (**1**) and (**2**) are considered as simple BH-equivalent three-orbital two-electron contributors, and the $Pt(PMe_2Ph)_2$ vertex in (**1**) is considered either as a BH_2^--equivalent *arachno*-type two-orbital two-electron contributor [structure (**IV**)] or as a BH^{2-}-equivalent three-orbital four-electron contributor, then both (**1**) and (**2**) could be regarded as members of the same *conjuncto* family notionally derived from the isomers of the B_nH_{n+4} binary borane $B_{17}H_{21}$. This last species is unknown at present, although its congeners $B_{16}H_{20}$, *syn*-$B_{18}H_{22}$, and *anti*-$B_{18}H_{22}$ are well characterized.[37,66–68] These species each consist of two open subclusters fused with an edge (two atoms) in common, and with the two open faces mutually non-facing. As such they have obvious structural parallels to the red species $[(PMe_2Ph)PtB_{16}H_{18}(PMe_2Ph)]$ (**2**) (Figure 6). The green species $[(PMe_2Ph)_4Pt_3B_{14}H_{18}]$ (**1**) (Figure 3), however, is less precedented in this context. The two-edge (three-atom, non-triangulated) *conjuncto* feature appears to have no parallels yet in binary boron hydride chemistry, although the mutually facing subcluster open faces do have a parallel in the smaller B_nH_{n+6} conjuncto species $B_{14}H_{20}$.[28,69] However, this type of comparison ignores the differential effects of orbital geometry between tetrahedral boron and orthogonal platinum, and also any additional cluster bonding participation from platinum valence-shell electrons, and so an extended discussion is not warranted.

Experimental

General.—The platinum complex *cis*-$[PtCl_2(PMe_2Ph)_2]$ was prepared from $K_2[PtCl_4]$ and PMe_2Ph by standard methods.

$B_{10}H_{14}$ was sublimed (0.1 mmHg/80 °C) before use and $[NEt_4][B_9H_{14}]$ was prepared from it by published methods.[27,64] $[(PMe_2Ph)_2PtB_8H_{12}]$ was prepared from *cis*-$[PtCl_2(PMe_2Ph)_2]$ and $[NEt_4][B_9H_{14}]$ by a literature method.[27] Toluene was refluxed over and distilled from Na before use and CH_2Cl_2 was refluxed over and distilled from CaH_2. Nitrogen gas was dried by passage through concentrated H_2SO_4 and then over KOH pellets.

Thermolysis of $[(PMe_2Ph)_2PtB_8H_{12}]$.—In a typical experiment $[(PMe_2Ph)_2PtB_8H_{12}]$ (100 mg, 1.2 mmol) was suspended in dry toluene (50 cm^3) which was refluxed under a flow of dry N_2 for 1 h. Under reflux the starting $[(PMe_2Ph)_2PtB_8H_{12}]$ dissolved completely and as the reflux continued the reaction solution darkened rapidly. The solvent was removed under reduced pressure (water pump) at 90 °C (water-bath) and the residue redissolved in dry CH_2Cl_2 (*ca.* 3 cm^3) and applied to a series of preparative t.l.c. plates (Kieselgel GF 254 Fluka AG) which were then eluted with CH_2Cl_2–light petroleum (b.p. 60—80 °C; 80:20). Several coloured bands were observed upon elution, the three most intense being a green component [R_f 0.6, compound (**1**)], a red component [R_f 0.7, compound (**2**)], and a yellow component [R_f 0.9, compound (**3**)]. These were separately removed from the plates and further purified by preparative t.l.c., initially using Et_2O–pentane (25:75), and then repeating the procedure with toluene (100%) as the eluants. Compounds (**1**), (**2**), and (**3**) were obtained pure (by n.m.r. spectroscopic analysis) in *ca.* 6, 2, and 4% yields respectively (based on platinum content). Crystals of (**1**) (as the 1:1 solvate with CH_2Cl_2) suitable for *X*-ray analysis were obtained by diffusion of hexane into solutions of (**1**) in CH_2Cl_2 at room temperature, and of (**2**) by recrystallization from hot cyclohexane. Compound (**3**) was identified as $[(PMe_2Ph)_2Pt_2B_{12}H_{18}]$ by comparison of its n.m.r. spectroscopic properties with those found in the literature.[28] Smaller quantities of other highly coloured compounds have also sometimes been obtained from this reaction and amongst these are three orange-red compounds (**4**), (**5**), and (**6**) with R_f values of *ca.* 0.3 in CH_2Cl_2–light petroleum (b.p. 60—80 °C) (80:20). Preliminary boron-11 and phosphorus-31 n.m.r. experiments showed these compounds were also macropolyhedral clusters [see Results and Discussion, section (*a*)] but unfortunately crystals suitable for single-crystal *X*-ray diffraction analysis have not yet been obtained from the small quantities of material available. The yield (and incidence) of these other species is erratic and may therefore depend on impurities at trace level in the starting $[(PMe_2Ph)_2PtB_8H_{12}]$.

Crystal Data for $[(PMe_2Ph)_4Pt_3B_{14}H_{16}]\cdot CH_2Cl_2$ (**1**).—$C_{33}H_{62}B_{14}Cl_2P_4Pt_3$, M = 1 390.3, monoclinic, a = 1 249.0(3), b = 3 732.6(8), c = 1 072.0(2) pm, β = 104.92(2)°, Z = 4, U = 4.828 8(15) nm^3, D_c = 1.912 g cm^{-3}, $F(000)$ = 2 632, space group $P2_1/c$, Mo-K_α radiation (graphite monochromatized), λ = 71.069 pm, μ(Mo-K_α) 9.0294 cm^{-1}. 4 802 Independent F_o with $I > 2\sigma(I)$.

Structure Determination of Compound (**1**).—The crystal used was regular with dimensions *ca.* 0.15 × 0.75 × 0.70 mm. The intensity measurements were made using a Syntex $P2_1$ diffractometer. Accurate cell dimensions and their standard deviations were obtained by least-squares treatment of the setting angles for 15 reflections having $35 < 2\theta < 40°$. Intensities of all independent reflections within the range $4 < 2\theta < 45°$ were measured in the ω—2θ scan mode with scan speeds varying between 3 and 29° min^{-1} according to a pre-scan intensity and running from 0.75° below $K_{\alpha1}$ to 0.75° above $K_{\alpha2}$. After correction for Lorentz, polarization, and transmission (T = 0.3012—0.4158) factors, the 4 802 reflections having $I > 2\sigma(I)$ were retained for the structure analysis; 869 below this threshold were rejected as 'unobserved'. The three Pt atoms were located from a Patterson map and the remaining non-hydrogen atoms were located from successive difference

Table 9. Fractional atomic co-ordinates for $[(PMe_2Ph)_4Pt_3B_{14}H_{16}]\cdot CH_2Cl_2$ (**1**)

Atom	*x*	*y*	*z*	Atom	*x*	*y*	*z*
Pt(10)	0.265 64(5)	0.140 80(2)	−0.141 00(5)	Me(31)	−0.211 3(13)	0.163 4(4)	0.171 1(16)
Pt(2)	0.032 68(5)	0.149 53(2)	0.045 38(6)	Me(32)	−0.237 0(12)	0.117 3(3)	−0.043 2(14)
Pt(7)	0.214 35(5)	0.094 25(2)	0.107 33(6)	Me(41)	0.048 7(12)	0.208 7(4)	0.313 0(16)
P(1)	0.351 1(3)	0.141 0(1)	−0.305 9(3)	Me(42)	0.165 8(13)	0.234 8(4)	0.134 8(16)
P(2)	0.231 0(3)	0.040 0(1)	0.214 4(3)	C(11)	0.419 9(8)	0.182 9(2)	−0.325 2(11)
P(4)	0.047 1(3)	0.206 0(1)	0.139 7(3)	C(12)	0.410 2(8)	0.212 6(2)	−0.249 8(11)
P(3)	−0.129 5(3)	0.131 4(1)	0.098 5(3)	C(13)	0.456 8(8)	0.245 3(2)	−0.270 8(11)
Cl(1)	0.314 5(6)	−0.060 1(3)	0.397 4(6)	C(14)	0.513 0(8)	0.248 3(2)	−0.367 2(11)
Cl(2)	0.327 5(6)	−0.123 5(2)	0.543 1(7)	C(15)	0.522 6(8)	0.218 6(2)	−0.442 6(11)
C	0.245 4(22)	−0.101 2(6)	0.428 3(25)	C(16)	0.476 1(8)	0.185 9(2)	−0.421 6(11)
B(1)	−0.009 2(13)	0.129 2(4)	−0.157 3(16)	C(21)	0.351 0(7)	0.013 9(2)	0.202 9(11)
B(3)	0.034 2(13)	0.092 4(4)	−0.036 5(16)	C(22)	0.342 5(7)	−0.009 0(2)	0.097 8(11)
B(4)	0.036 2(14)	0.088 5(4)	−0.202 4(17)	C(23)	0.435 9(7)	−0.027 1(2)	0.082 4(11)
B(5)	0.088 4(14)	0.129 8(4)	−0.252 3(17)	C(24)	0.537 9(7)	−0.022 4(2)	0.172 2(11)
B(6)	0.104 9(13)	0.163 1(4)	−0.120 6(16)	C(25)	0.546 4(7)	0.000 4(2)	0.277 3(11)
B(8)	0.141 1(14)	0.065 7(4)	−0.084 4(17)	C(26)	0.453 0(7)	0.018 6(2)	0.292 6(11)
B(9)	0.173 0(13)	0.089 4(4)	−0.217 4(16)	C(31)	−0.107 6(8)	0.093 8(2)	0.213 7(8)
B(11)	0.201 6(13)	0.146 2(4)	0.023 2(16)	C(32)	−0.166 2(8)	0.061 8(2)	0.185 7(3)
B(1′)	0.437 5(13)	0.150 5(4)	0.171 6(16)	C(33)	−0.153 5(8)	0.035 1(2)	0.279 7(8)
B(5′)	0.387 3(13)	0.110 2(4)	0.217 0(16)	C(34)	−0.082 0(8)	0.040 6(2)	0.401 7(8)
B(2′)	0.295 4(12)	0.147 4(3)	0.180 8(14)	C(35)	−0.023 4(8)	0.072 6(2)	0.429 7(8)
B(3′)	0.329 5(12)	0.171 9(3)	0.046 7(14)	C(36)	−0.036 1(8)	0.099 3(2)	0.335 7(8)
B(9′)	0.435 6(14)	0.147 4(4)	0.005 2(17)	C(41)	−0.067 4(6)	0.234 6(2)	0.055 9(9)
B(4′)	0.481 1(13)	0.111 4(4)	0.117 9(16)	C(42)	−0.083 9(6)	0.268 1(2)	0.105 2(9)
Me(11)	0.253 7(13)	0.135 6(4)	−0.465 7(16)	C(43)	−0.170 3(6)	0.290 0(2)	0.038 3(9)
Me(12)	0.454 0(13)	0.105 7(4)	−0.308 6(17)	C(44)	−0.240 1(6)	0.278 3(2)	−0.078 1(9)
Me(21)	0.248 0(12)	0.043 7(3)	0.390 7(14)	C(45)	−0.223 6(6)	0.244 8(2)	−0.127 4(9)
Me(22)	0.113 3(13)	0.008 0(4)	0.167 3(16)	C(46)	−0.137 3(6)	0.222 9(2)	−0.060 5(9)

Table 10. Fractional atomic co-ordinates for $[(PMe_2Ph)PtB_{16}H_{18}(PMe_2Ph)]$ (**2**)

Atom	*x*	*y*	*z*	Atom	*x*	*y*	*z*
Pt(7)	−0.234 28(3)	−0.2500	−0.241 02(2)	H(111)	0.122 4(10)	−0.177 3(11)	−0.217 6(8)
P(1)	−0.095 0(4)	−0.075 1(4)	−0.223 7(4)	H(112)	0.084 0(10)	−0.129 2(11)	−0.100 8(8)
P(2)	−0.568 0(2)	−0.543 6(2)	−0.112 2(2)	H(113)	0.138 6(10)	−0.018 3(11)	−0.183 7(9)
B(1)	−0.535 0(10)	−0.208 4(10)	−0.391 5(7)	Me(12)	−0.148 1(12)	0.050 5(11)	−0.147 6(8)
B(2)	−0.459 3(8)	−0.252 5(20)	−0.273 5(6)	H(121)	−0.252 1(12)	0.074 5(11)	−0.169 6(8)
B(3)	−0.524 9(11)	−0.367 5(11)	−0.353 4(8)	H(122)	−0.084 7(12)	0.131 5(11)	−0.155 4(8)
B(4)	−0.493 8(14)	−0.322 3(12)	−0.474 2(9)	H(123)	−0.139 4(12)	0.020 6(11)	−0.072 5(8)
B(5)	−0.405 0(14)	−0.177 2(13)	−0.467 8(9)	Me(21)	−0.552 8(11)	−0.602 8(11)	0.010 8(8)
B(6)	−0.380 3(11)	−0.135 2(11)	−0.341 6(8)	H(211)	−0.510 1(11)	−0.531 2(11)	0.059 6(8)
B(8)	−0.386 9(11)	−0.403 9(12)	−0.252 1(8)	H(212)	−0.487 6(11)	−0.684 1(11)	0.015 2(8)
B(1′)	−0.148 9(11)	−0.560 9(11)	−0.224 7(8)	H(213)	−0.651 5(11)	−0.625 7(11)	0.031 3(8)
B(2′)	−0.228 5(10)	−0.443 8(11)	−0.302 3(7)	Me(22)	−0.694 4(10)	−0.420 2(11)	−0.113 5(7)
B(3′)	−0.328 9(10)	−0.558 8(11)	−0.254 0(7)	H(221)	−0.709 0(10)	−0.380 0(11)	−0.185 5(7)
B(4′)	−0.260 4(11)	−0.586 3(12)	−0.130 4(8)	H(222)	−0.660 5(10)	−0.348 4(11)	−0.061 8(7)
B(5′)	−0.107 5(12)	−0.499 0(11)	−0.107 5(9)	H(223)	−0.788 7(10)	−0.459 0(11)	−0.093 9(7)
B(6′)	−0.085 4(22)	−0.406 4(17)	−0.209 1(14)	C(11)	−0.083 5(7)	−0.004 5(6)	−0.341 9(4)
B(9′)	−0.399 2(10)	−0.485 9(11)	−0.153 5(7)	C(12)	−0.016 3(7)	−0.073 3(6)	−0.408 9(4)
B(10′)	−0.260 1(10)	−0.449 7(11)	−0.057 1(8)	C(13)	−0.011 4(7)	−0.029 0(6)	−0.503 7(4)
B(11′)	−0.136 9(11)	−0.338 0(11)	−0.100 0(8)	C(14)	−0.073 7(7)	0.084 2(6)	−0.531 5(4)
H(1)	−0.632 7(102)	−0.160 7(105)	−0.400 3(69)	C(15)	−0.140 9(7)	0.153 0(6)	−0.464 5(4)
H(2)	−0.506 3(85)	−0.215 5(102)	−0.206 7(63)	C(16)	−0.145 8(7)	0.108 7(6)	−0.369 7(4)
H(3)	−0.615 0(106)	−0.429 2(113)	−0.353 1(71)	H(12)	0.031 9(7)	−0.160 9(6)	−0.387 3(4)
H(3,4)	−0.468 6(105)	−0.399 8(110)	−0.429 4(77)	H(13)	0.040 6(7)	−0.082 2(6)	−0.555 5(4)
H(4)	−0.536 3(103)	−0.351 6(105)	−0.547 5(79)	H(14)	−0.069 9(7)	0.118 5(6)	−0.604 9(4)
H(4,5)	−0.386 8(90)	−0.253 3(169)	−0.495 5(67)	H(15)	−0.189 1(7)	0.240 6(6)	−0.486 1(4)
H(5)	−0.386 3(102)	−0.110 8(104)	−0.528 9(75)	H(16)	−0.197 8(7)	0.162 0(6)	−0.317 9(4)
H(5,6)	−0.311 3(104)	−0.167 6(104)	−0.422 8(73)	C(21)	−0.639 2(7)	−0.668 3(5)	−0.187 2(5)
H(6)	−0.401 2(102)	−0.009 6(107)	−0.332 1(75)	C(22)	−0.568 0(7)	−0.781 0(5)	−0.187 5(5)
H(1′)	−0.095 8(100)	−0.651 6(104)	−0.257 1(70)	C(23)	−0.616 0(7)	−0.878 8(5)	−0.248 2(5)
H(2′)	−0.210 0(99)	−0.449 9(104)	−0.389 7(71)	C(24)	−0.735 1(7)	−0.863 8(5)	−0.308 8(5)
H(3′)	−0.380 0(101)	−0.640 6(105)	−0.302 0(71)	C(25)	−0.806 3(7)	−0.751 1(5)	−0.308 5(5)
H(4′)	−0.267 5(99)	−0.681 7(97)	−0.089 0(69)	C(26)	−0.758 3(7)	−0.653 4(5)	−0.247 8(5)
H(5′)	−0.018 2(103)	−0.536 5(108)	−0.054 0(71)	H(22)	−0.475 8(7)	−0.792 6(5)	−0.140 6(5)
H(6′)	0.030 9(106)	−0.394 1(106)	−0.228 9(74)	H(23)	−0.560 9(7)	−0.966 0(5)	−0.248 4(5)
H(10′)	−0.273 0(98)	−0.463 8(102)	−0.021 8(73)	H(24)	−0.772 3(7)	−0.939 5(5)	−0.355 8(5)
H(10′,11′)	−0.259 6(105)	−0.349 8(110)	−0.078 2(76)	H(25)	−0.898 6(7)	−0.739 5(5)	−0.355 4(5)
H(11′)	−0.071 7(81)	−0.226 5(134)	−0.051 0(60)	H(26)	−0.813 4(7)	−0.566 1(5)	−0.247 6(5)
Me(11)	0.080 4(10)	−0.102 8(11)	−0.176 6(8)				

syntheses. Full-matrix least-squares refinement, with anisotropic thermal parameters for Pt and P, and isotropic for all the remaining non-hydrogen atoms, led to a convergence with R = 0.049, R' = 0.045. The phenyl rings were included in the refinement as rigid groups (C–C 139.5 pm, C–C–C 120°) as allowed by the SHELX programs.[70] The least-squares weights were obtained from counting statistics such that $w^{-1} = \sigma^2(F_o)$. Final atomic co-ordinates are given in Table 9.

Crystal Data for $[(PMe_2Ph)PtB_{16}H_{18}(PMe_2Ph)]$ (**2**).—$C_{16}H_{40}B_{16}P_2Pt$, M = 622.5, monoclinic, space group $P2_1$, a = 992.7(3), b = 1 067.2(2), c = 1 378.7(3) pm, β = 95.08(2)°, U = 1 454 9(5) nm^3, Z = 2, D_c = 1.512 g cm^{-3}, $F(000)$ = 648, Mo-K_α radiation (graphite monochromatized), λ = 71.069 pm, μ(Mo-K_α) 49.87 cm^{-1}. 1 992 Independent F_o with $I > 2\sigma(I)$.

Structure Determination of Compound (**2**).—All crystallographic measurements were made on a Syntex $P2_1$ diffractometer. Accurate cell dimensions and their standard deviations were obtained by least-squares treatment of the setting angles of 15 reflections with $35 < 2\theta < 40°$. The intensities of the 2 043 independent reflections in the range $4 < 2\theta < 45°$ were measured in the ω—2θ scan mode. Variable scan speeds of between 2 and 29° min^{-1} were used and each scan ran from 1° below $K_{\alpha1}$ to 1° above $K_{\alpha2}$. After correction for Lorentz, polarization, and transmission factors the 1 992 reflections with $I > 2\sigma(I)$ were retained for the structure analysis. The structure was determined by standard heavy-atom procedures and refined by full-matrix least squares using the SHELX system of programs.[70] The Pt atom was assigned anisotropic thermal parameters while all the other atoms were refined with individual isotropic thermal parameters. The phenyl rings were included in the refinement as rigid groups with hexagonal symmetry (C–C = 139.5 pm). All the phenyl and methyl hydrogens were included in calculated positions (C–H = 108 pm). All other hydrogen atoms were located experimentally and refined freely with individual isotropic thermal parameters. A weighting scheme of the form $w^{-1} = \sigma^2(F_o)$ was used to give acceptable analyses. Final R values are R = 0.0216 and R' = 0.0248. Refinement of the inverse structure gave a higher R value (R = 0.036 for inverse, R = 0.030 for accepted structure, no hydrogen atoms included in refinements) and was rejected on this basis. Table 10 lists the atomic co-ordinates.

Nuclear Magnetic Resonance Spectroscopy.—100-MHz ^{1}H and ^{1}H-{^{11}B}, 32-MHz ^{11}B and ^{11}B-{^{1}H}, and 40-MHz ^{31}P-{^{1}H} experiments were carried out on a JEOL FX-100 pulse (Fourier-transform) spectrometer. High-field (128-MHz) ^{11}B and ^{11}B-{^{1}H} experiments were performed on a Bruker WH-400 pulse (Fourier-transform) spectrometer (S.E.R.C. Service, University of Sheffield) and high-field (360-MHz) ^{1}H-{^{11}B} experiments were performed on a Bruker WH-360 spectrometer (S.E.R.C. Service, University of Edinburgh).

Solutions and conditions are specified in Tables 5—8. Chemical shifts (δ) are given in p.p.m. to high frequency (low field) of $SiMe_4$ for ^1H, of $BF_3(OEt_2)$ in $CDCl_3$ [Ξ 32 083 971 Hz][48] for ^{11}B, and of 85% H_3PO_4 [Ξ 40 480 730 Hz] for ^{31}P. The general technique for selective ^1H-{^{11}B} n.m.r. spectroscopy has been discussed elsewhere.[27,50,51] ^{31}P Spectra were generally recorded at lower temperatures to maximize 'thermal decoupling' of ^{10}B and ^{11}B.[49] Two-dimensional ^{11}B homonuclear boron–boron correlation spectroscopy (COSY) was performed at 128 MHz on a Bruker WH-400 spectrometer (S.E.R.C. Service, University of Warwick). General aspects of the technique as used in the present work are to be presented elsewhere.

Acknowledgements

We thank Dr. D. Reed (University of Edinburgh) and Dr. O. Howarth (University of Warwick) for services in high-field n.m.r. spectroscopy, Dr. M. Thornton-Pett for crystallographic assistance, Johnson Matthey Ltd. for the loan of chemicals, and the S.E.R.C. for support.

References

1 K. Wade, *Chem. Commun.*, 1971, 792.
2 K. Wade, *Adv. Inorg. Chem. Radiochem.*, 1976, **18**, 1.
3 R. E. Williams, *Inorg. Chem.*, 1971, **10**, 210.
4 D. M. P. Mingos, *Nature (London), Phys. Sci.*, 1972, **236**, 99.
5 R. Mason, K. M. Thomas, and D. M. P. Mingos, *J. Am. Chem. Soc.*, 1973, **95**, 3802.
6 R. W. Rudolph, *Acc. Chem. Res.*, 1976, **9**, 446 and refs. therein.
7 See, for example, M. E. O'Neill and K. Wade, in 'Metal Interactions with Boron Clusters,' ed. R. N. Grimes, Plenum Press, New York and London, 1982, ch. 1, pp. 1—41.
8 D. G. Evans and D. M. P. Mingos, *Organometallics*, 1983, **2**, 435 and refs. therein.
9 D. M. P. Mingos, *Acc. Chem. Res.*, 1984, **17**, 311 and refs. therein.
10 M. A. Beckett, J. E. Crook, N. N. Greenwood, and J. D. Kennedy, *J. Chem. Soc., Dalton Trans.*, 1984, 1427.
11 J. Bould, J. E. Crook, N. N. Greenwood, and J. D. Kennedy, *J. Chem. Soc., Dalton Trans.*, 1984, 1903.
12 R. N. Grimes, in 'Comprehensive Organometallic Chemistry,' eds. G. Wilkinson, F. G. A. Stone, and E. Abel, Pergamon Press, Oxford, 1982, Part 1, ch. 5.5.
13 K. B. Gilbert, S. K. Boocock, and S. G. Shore, in 'Comprehensive Organometallic Chemistry,' eds. G. Wilkinson, F. G. A. Stone, and E. Abel, Pergamon Press, Oxford, 1982, Part 6, ch. 41.
14 K. Housecroft and T. P. Fehlner, *Adv. Organomet. Chem.*, 1982, **21**, 59.
15 N. N. Greenwood, *Pure Appl. Chem.*, 1983, **55**, 77.
16 J. D. Kennedy, *Prog. Inorg. Chem.*, 1984, **32**, 579; in the press and refs. therein.
17 N. N. Greenwood, *Chem. Soc. Rev.*, 1984, **13**, 353.
18 J. Bould, Ph.D. Thesis, University of Leeds, 1983.
19 J. Bould, N. N. Greenwood, J. D. Kennedy, and W. S. McDonald, *J. Chem. Soc., Dalton Trans.*, 1985, 1843.
20 J. E. Crook, M. Elrington, N. N. Greenwood, J. D. Kennedy, and J. D. Woollins, *Polyhedron*, 1984, **3**, 901.
21 J. E. Crook, M. Elrington, N. N. Greenwood, J. D. Kennedy, M. Thornton-Pett, and J. D. Woollins, *J. Chem. Soc., Dalton Trans.*, 1985, 2407.
22 H. Fowkes, N. N. Greenwood, J. D. Kennedy, and M. Thornton-Pett, *J. Chem. Soc., Dalton Trans.*, 1986, 517.
23 M. A. Beckett, J. E. Crook, N. N. Greenwood, J. D. Kennedy, and W. S. McDonald, *J. Chem. Soc., Chem. Commun.*, 1982, 552.
24 M. A. Beckett, J. E. Crook, N. N. Greenwood, and J. D. Kennedy, *J. Chem. Soc., Chem. Commun.*, 1983, 1228.
25 M. A. Beckett, Abstracts 5th Internat. Meeting Boron Chemistry, IMEBORON V, Swansea, 1983, Abstract no. CA15.
26 M. A. Beckett, N. N. Greenwood, and J. D. Kennedy, Abstracts 2nd Internat. Meeting Chemistry of Platinum Metals, Edinburgh, 1984, Abstract no. A26.
27 S. K. Boocock, N. N. Greenwood, M. J. Hails, J. D. Kennedy, and W. S. McDonald, *J. Chem. Soc., Dalton Trans.*, 1981, 1415.
28 N. N. Greenwood, M. J. Hails, J. D. Kennedy, and W. S. McDonald, *J. Chem. Soc., Chem. Commun.*, 1980, 37; *J. Chem. Soc., Dalton Trans.*, 1985, 953.
29 R. Ahmad, J. E. Crook, N. N. Greenwood, and J. D. Kennedy, *J. Chem. Soc., Dalton Trans.*, in the press.
30 J. E. Crook, N. N. Greenwood, J. D. Kennedy, and W. S. McDonald, *J. Chem. Soc., Dalton Trans.*, 1984, 2487.
31 J. Bould, N. N. Greenwood, and J. D. Kennedy, *Polyhedron*, 1983, **2**, 1401.
32 C. T. Brewer and R. N. Grimes, *J. Am. Chem. Soc.*, 1984, **106**, 2722; C. T. Brewer, R. G. Swisher, E. Sinn, and R. N. Grimes, *ibid.*, 1985, **107**, 3558; see also, C. T. Brewer and R. N. Grimes, *ibid.*, p. 3552.
33 J. Plešek, S. Heřmánek, B. Štíbr, and F. Hanousek, *Collect. Czech. Chem. Commun.*, 1967, **32**, 1095.
34 J. Plešek, S. Heřmánek, and F. Hanousek, *Collect. Czech. Chem. Commun.*, 1968, **33**, 699.
35 J. Bould, J. E. Crook, N. N. Greenwood, J. D. Kennedy, and W. S. McDonald, *J. Chem. Soc., Chem. Commun.*, 1982, 346.
36 J. Bould, N. N. Greenwood, and J. D. Kennedy, *J. Chem. Soc., Dalton Trans.*, 1984, 2477.
37 L. Barton, in 'Topics in Current Chemistry—100. New Trends in Chemistry,' ed. F. L. Boschke, Springer, Berlin, Heidelberg, and New York, 1982, pp. 169—206.
38 N. N. Greenwood and B. S. Thomas, in 'Comprehensive Inorganic Chemistry,' eds. J. C. Bailar, H. J. Emeleus, R. Nyholm, and A. F. Trotman-Dickenson, Pergamon Press, Oxford, 1983, pp. 665—991.
39 S. K. Boocock, N. N. Greenwood, J. D. Kennedy, W. S. McDonald, and J. Staves, *J. Chem. Soc., Dalton Trans.*, 1981, 2573.
40 M. A. Beckett, N. N. Greenwood, J. D. Kennedy, and M. Thornton-Pett, *Polyhedron*, 1985, **4**, 505.
41 J. Bould, J. E. Crook, N. N. Greenwood, and J. D. Kennedy, *J. Chem. Soc., Chem. Commun.*, 1983, 943.
42 Y. M. Cheek, N. N. Greenwood, J. D. Kennedy, and W. S. McDonald, *J. Chem. Soc., Chem. Commun.*, 1982, 80.
43 M. Green, J. L. Spencer, and F. G. A. Stone, *J. Chem. Soc., Dalton Trans.*, 1979, 1679.
44 M. A. Beckett, N. N. Greenwood, J. D. Kennedy, and M. Thornton-Pett, *J. Chem. Soc., Dalton Trans.*, 1985, 1119.
45 N. N. Greenwood, J. D. Kennedy, M. Thornton-Pett, and J. D. Woollins, *J. Chem. Soc., Dalton Trans.*, 1985, 2397.
46 R. Ahmad, J. E. Crook, N. N. Greenwood, J. D. Kennedy, and W. S. McDonald, *J. Chem. Soc., Chem. Commun.*, 1982, 1019.
47 J. Bould, J. E. Crook, N. N. Greenwood, and J. D. Kennedy, *J. Chem. Soc., Chem. Commun.*, 1983, 951.
48 J. D. Kennedy, in 'Multinuclear NMR (NMR in Inorganic and Organometallic Chemistry),' ed. J. Mason, Plenum Press, London and New York, in the press and refs. therein.
49 J. D. Kennedy and J. Staves, *Z. Naturforsch., Teil B*, 1979, **34**, 808.
50 J. D. Kennedy and N. N. Greenwood, *Inorg. Chim. Acta*, 1980, **38**, 93.
51 J. D. Kennedy and B. Wrackmeyer, *J. Magn. Reson.*, 1980, **38**, 529.
52 R. F. Sprecher and J. C. Carter, *J. Am. Chem. Soc.*, 1973, **95**, 2369.
53 B. E. Aufderheide and R. F. Sprecher, *Inorg. Chem.*, 1974, **13**, 228.
54 R. E. Sprecher and B. E. Aufderheide, *Inorg. Chem.*, 1974, **13**, 2287.
55 R. E. Sprecher, B. E. Aufderheide, G. W. Luther, and J. C. Carter, *J. Am. Chem. Soc.*, 1974, **96**, 4404.
56 F. S. Swicker, *Diss. Abstr. Int. B*, 1972, **32**, 4474.
57 J. Jeener, results communicated to the Ampere International Summer School, Basko Polje, Yugoslavia, 1971.
58 I. J. Colquhoun and W. McFarlane, results communicated to the First National Meeting of British Inorganic Boron Chemists, INTRABORON I, Strathclyde, May, 1980, and the Third Meeting, INTRABORON III, Leeds, September 1982; and as cited in ref. 48.
59 T. L. Venable, W. C. Hutton, and R. N. Grimes, *J. Am. Chem. Soc.*, 1982, **104**, 4716.
60 D. Reed, *J. Chem. Res. (S)*, 1984, 198.
61 T. L. Venable, W. C. Hutton, and R. N. Grimes, *J. Am. Chem. Soc.*, 1984, **106**, 29.
62 M. Jasztal, results communicated to the Fourth National Meeting of British Inorganic Boron Chemists, INTRABORON IV, Durham, September 1984.
63 D. Meina, results communicated to INTRABORON IV, Durham, September 1984.

64 X. L. R. Fontaine, H. Fowkes, N. N. Greenwood, J. D. Kennedy, and M. Thornton-Pett, *J. Chem. Soc., Dalton Trans.*, 1986, 547.
65 R. Ahmad, Ph.D. Thesis, University of Leeds, 1982.
66 L. B. Friedman, R. E. Cook, and M. D. Glick, *Inorg. Chem.*, 1970, **9**, 1452.
67 P. G. Simpson and W. N. Lipscomb, *J. Chem. Phys.*, 1963, **30**, 2339.
68 P. G. Simpson, K. Folting, R. D. Dobrott, and W. N. Lipscomb, *J. Chem. Phys.*, 1963, **30**, 2339.
69 J. C. Huffman, D. C. Moody, and R. Schaeffer, *J. Am. Chem. Soc.*, 1970, **97**, 1621.
70 G. M. Sheldrick, SHELX 76, Program system for *X*-ray structure determination, University of Cambridge, 1976.

Received 31*st July* 1985; *Paper* 5/1331